# Low temperature aqueous alteration of basalt: Mineral assemblages of Deccan basalts and implications for Mars

R. N. Greenberger,[1] J. F. Mustard,[1] P. S. Kumar,[2] M. D. Dyar,[3] E. A. Breves,[3] and E. C. Sklute[4]

Received 11 May 2012; revised 18 July 2012; accepted 4 August 2012; published 18 September 2012.

[1] Al-rich phyllosilicates (kaolinite, montmorillonite) have been found in layers overlying Fe/Mg-smectites on Mars, and it has been suggested that this stratigraphy formed through in situ leaching at the surface, similar to terrestrial weathering profiles. We are investigating the remotely sensed signatures of this type of weathering using ten samples from a vertical section of altered Deccan basalts and four samples collected nearby as an analog for leaching resulting in Al-rich phyllosilicate over Fe/Mg-smectite stratigraphies. Samples were analyzed with reflectance spectroscopy from 0.28 to 25.0 $\mu$m, inductively coupled plasma atomic emission spectrometry for 10 major element concentrations (Al, Ca, Fe, K, Mg, Mn, Na, P, Si, Ti), loss on ignition for volatiles, x-ray diffraction (XRD) for mineralogies, and Mössbauer spectroscopy for Fe redox state. Spectra of basalt samples were dominated by $Fe^{2+}$ crystal field transitions with weak alteration bands near 1.4 and/or 1.9 $\mu$m. Reststrahlen bands in mid-infrared showed the convolution of plagioclase and pyroxene features typical of basalts. Saprolite samples were incompletely leached, and their spectra were dominated by complex Al- and Fe/Mg-bearing smectite clays and retained no original mafic signatures. XRD and Mössbauer detected pyroxene and plagioclase not visible by reflectance spectroscopy in some saprolite samples. Zeolites were present throughout the saprolite. The laterite was the most leached horizon, and all analyses showed kaolinite and iron oxide assemblages. This kaolinite and hematite association would be expected if kaolinite on Mars formed through leaching under conditions similar to those on Earth and has implications for abundant freshwater on the Martian surface.

**Citation:** Greenberger, R. N., J. F. Mustard, P. S. Kumar, M. D. Dyar, E. A. Breves, and E. C. Sklute (2012), Low temperature aqueous alteration of basalt: Mineral assemblages of Deccan basalts and implications for Mars, *J. Geophys. Res.*, *117*, E00J12, doi:10.1029/2012JE004127.

## 1. Introduction

[2] Hydrated silicates such as phyllosilicates formed early on Mars through aqueous alteration of the basaltic crust and have been detected by the Compact Reconnaissance Imaging Spectrometer for Mars (CRISM) and Observatoire pour la Minéralogie, l'Eau, les Glaces et l'Activité (OMEGA) [e.g., *Bibring et al.*, 2005; *Mustard et al.*, 2008]. These minerals formed when liquid water interacted with and altered the Martian crust deep in the subsurface, in the shallow subsurface, in hydrothermal systems, and at the surface [*Murchie et al.*, 2009]. It has been suggested that phyllosilicates formed early in Mars' history, and then sulfates formed under more acidic conditions at lower water:rock ratios [*Bibring et al.*, 2006; *Ehlmann et al.*, 2011].

[3] Crustal sections exposed in impact craters and scarps enriched in Fe/Mg-smectite clays are common on Mars [e.g., *Murchie et al.*, 2009; *Mustard et al.*, 2008] and are sometimes overlain by a thin layer enriched in Al-phyllosilicates [e.g., *Ehlmann et al.*, 2009; *Murchie et al.*, 2009]. The term Al-phyllosilicate here refers to the most Al-rich phyllosilicates, such as kaolinite and montmorillonite, although there is Al present in other phyllosilicates. This Al-phyllosilicate over Fe/Mg-smectite stratigraphy has been found in two main regions: Nili Fossae and Mawrth Vallis [e.g., *Ehlmann et al.*, 2009; *Loizeau et al.*, 2007]. In eastern Nili Fossae, kaolinite has been detected in layers tens of meters thick on top of Fe/Mg smectite-bearing units [*Ehlmann et al.*, 2009]. In Mawrth Vallis, extensive layers of kaolinite and montmorillonite have been found overlying Fe/Mg smectite-bearing units, in places with hydrated silica or possible $Fe^{2+}$-

[1]Department of Geological Sciences, Brown University, Providence, Rhode Island, USA.
[2]National Geophysical Research Institute, Council of Scientific & Industrial Research, Hyderabad, India.
[3]Department of Astronomy, Mount Holyoke College, South Hadley, Massachusetts, USA.
[4]Department of Geosciences, State University of New York at Stony Brook, Stony Brook, New York, USA.

Corresponding author: R. N. Greenberger, Department of Geological Sciences, Brown University, Providence, RI 02912, USA. (rebecca_greenberger@brown.edu)


0148-0227/12/2012JE004127

bearing clays in the middle, and this region was proposed as a landing site for the Mars Science Laboratory Curiosity rover [e.g., *Bishop et al.*, 2008a; *Loizeau et al.*, 2007; *McKeown et al.*, 2009; *Wray et al.*, 2009]. The Al-phyllosilicate-bearing layers in Mawrth Vallis may drape topography and thus would have formed after the outflow channel [*Bishop et al.*, 2008a; *Howard and Moore*, 2007; *Wray et al.*, 2008], or may predate the channel [*Loizeau et al.*, 2007; *Michalski and Noe Dobrea*, 2007].

[4] The consistent nature of this Al-phyllosilicate-bearing over Fe/Mg-smectite-bearing stratigraphy has led to several formation hypotheses. One of the leading hypotheses is that this stratigraphy formed through in situ leaching or pedogenesis at the surface that altered the Fe/Mg-smectites to kaolinite or montmorillonite [*Bishop et al.*, 2008a; *Ehlmann et al.*, 2009; *Loizeau et al.*, 2007; *Mangold et al.*, 2007; *McKeown et al.*, 2009; *Noe Dobrea et al.*, 2010; *Wray et al.*, 2008]. On Earth, kaolinite can form through leaching of smectite and removal of a sheet of silica tetrahedra [e.g., *Jackson and Sherman*, 1953; *Rai and Kittrick*, 1989; *Righi and Meunier*, 1995]. This kaolinite over smectite stratigraphy is often seen in weathering profiles [e.g., *Nesbitt and Young*, 1989] and is commonly invoked to explain the observations on Mars. Several other hypotheses have also been suggested. Al-phyllosilicates could form through alteration of volcanic ash, which could explain the draping nature of some of the deposits [*Bishop et al.*, 2008a; *Loizeau et al.*, 2007; *McKeown et al.*, 2009; *Noe Dobrea et al.*, 2010]. Hydrothermal systems, possibly generated by an impact or emplacement of the overlying capping unit, may have led to the formation of kaolinite [*Ehlmann et al.*, 2009; *Schwenzer and Kring*, 2009]. Al-phyllosilicates could have formed elsewhere and been transported to their current location, as suggested by the layered nature of the deposits, so the kaolinite layer is from a different source region than the underlying Fe/Mg smectite [*Loizeau et al.*, 2007; *Michalski and Noe Dobrea*, 2007; *Wray et al.*, 2008]. Kaolinite and montmorillonite layers could have been created by interaction of layered phyllosilicates with the acidic solutions from which nearby sulfates precipitated [*Altheide et al.*, 2010]. In this scenario, the Al-phyllosilicates would have formed during a later period on Mars dominated by alteration at low pH [*Bibring et al.*, 2006]. Al-phyllosilicates may have formed through alteration of dust in small pockets of acidic brines within ice deposits or through leaching from basal melting of the ice [*Michalski and Niles*, 2011; *Niles and Michalski*, 2009a, 2009b], though this model presents problems in generating the volumes observed in an efficient manner. Al-phyllosilicates have been found in other types of deposits that are not overlying Fe/Mg smectite, such as in Columbus Crater where kaolinite may have precipitated out of a lake [e.g., *Wray et al.*, 2009], although these deposits are not the focus of this paper.

[5] Basaltic terrains have been identified across Mars, so it is important to have a well-characterized stratigraphy of altered basalts on Earth to test the leaching hypothesis for the formation of Al-phyllosilicates on Mars. The Deccan basalts are a good mid-infrared analog to basaltic terrains on Mars [*Christensen et al.*, 2000b]. After these basalts were emplaced 69–61 Ma [*Pande*, 2002], they were extensively altered and leached in place in a warm and wet climate as India passed through the equator to form deep weathering profiles and laterites [*Kısakürek et al.*, 2004; *Widdowson and Cox*, 1996]. Paleomagnetic data show that the laterites formed within 10–20 My after the lavas were emplaced [*Schmidt et al.*, 1983], and formation probably stopped when India collided with Asia and the region was uplifted [*Kısakürek et al.*, 2004]. What is left unexamined is how these alteration products and their mineral assemblages translate to spectroscopy and interpretation of their formational processes on Mars. The purpose of this paper is to characterize samples from a vertical section of altered Deccan basalts with laboratory analyses and connect their changing chemistries and mineralogies as a function of varying degrees of leaching to their spectroscopic signatures.

## 2. Background

[6] On Earth, smectite clays tend to form earlier in alteration sequences than kaolinite [e.g., *Jackson and Sherman*, 1953; *Nesbitt and Young*, 1989]. Fluids with higher silica and base cation activities and lower water:rock ratios are more conducive to forming smectites, while fluids with low silica and base cation activities and high water:rock ratios promote the formation of kaolinite [*Borchardt*, 1989; *Wilson*, 1999]. Thus, smectite tends to be favored in areas with poor drainage, and kaolinite is generally found in well-drained soils [*Borchardt*, 1989]. On Earth, smectites form in climates with low rainfall and dry periods with high evaporation because an impermeable layer forms from desiccation of the clays, decreasing drainage and increasing $SiO_2$ and base cations in solution [*Righi and Meunier*, 1995]. Kaolinite forms in regions with high rainfall throughout the year because this high volume of water promotes soil solutions with low $SiO_2$ and low base cations [*Righi and Meunier*, 1995]. In contrast, halloysite, a kaolin-group mineral, forms in arid climates with wet and dry cycles because kinetic factors prevent the formation of smectite [*Ziegler et al.*, 2003]. The CRISM observations of kaolin-group minerals currently do not distinguish between halloysite and kaolinite.

[7] Typical weathering profiles on Earth form through in situ leaching as a weathering front propagates into the subsurface and alters the parent rock [*White*, 1995]. Minerals most susceptible to weathering, such as olivine and anorthite, are altered first followed by more resistant minerals, such as quartz and K-feldspar [*Goldich*, 1938; *Nesbitt and Wilson*, 1992; *Wilson*, 2004]. The resulting profiles have unweathered material at the base and progressively more altered material higher in the profile [*Nesbitt and Wilson*, 1992]. In profiles developed on basalt, the basalt is weathered to smectite, then kaolinite [e.g., *Nesbitt and Young*, 1989], leading to a kaolinite over smectite stratigraphy similar to that seen on Mars. Under conditions of intense leaching and alteration in an oxidizing environment, an Fe-enriched laterite can form that generally has a kaolinite or gibbsite and Fe oxide assemblage [e.g., *Bourman and Ollier*, 2002; *Schellmann*, 1981].

[8] Terrestrial analogs can be used to better understand processes on Mars. Some previous analog studies looked at Hawaiian basalts and their alteration products [*Bishop et al.*, 2007; *Chemtob et al.*, 2010; *Minitti et al.*, 2007; *Seelos et al.*, 2010], alteration of basalts in a cold and wet climate or under hydrothermal conditions in Iceland [*Bishop et al.*, 2002b;

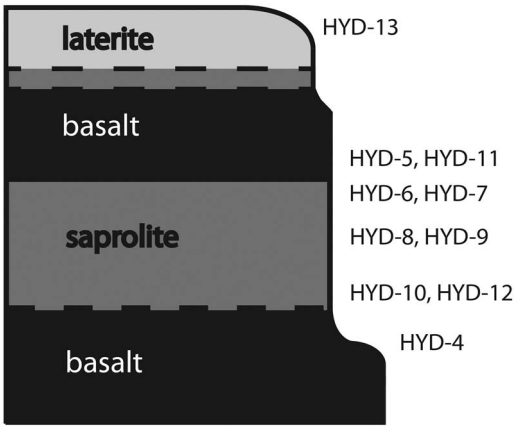


**Figure 1.** Representational stratigraphic section showing sampling locations. Due to the lack of any outcrop in some portions of the section, the thicknesses of layers are not to scale. The total thickness of the section is approximately 50 m. A saprolite was inferred to exist between the upper basalt layer and the laterite but could not be confirmed due to the lack of any outcrop.

*Ehlmann et al.*, 2012], hydrothermal and low temperature aqueous alteration of basalt in Svalbard, Norway [*Hausrath et al.*, 2008a, 2008b], phyllosilicates in Deccan bole beds [*Gavin et al.*, 2012], and alteration in the cold, dry climate of the Antarctic Dry Valleys (M. R. Salvatore et al., Initial stages of rock weathering in cold desert environments: Development of alteration rinds by oxidation-driven alteration processes and products in Beacon Valley, Antarctica, submitted to *Geochimica et Cosmochimica Acta*, 2012). The results of these studies include the characterization of the products of alteration of basalt in different environments and their spectral signatures. A complementary analog study focused on a weathering profile developed on serpentinized peridotite in Australia for comparison with the kaolinite over Fe/Mg-smectite stratigraphy on Mars and provides an excellent analysis of the mineral evolution of the profile upward and the implications for leaching on Mars [*Gaudin et al.*, 2011]. Our work characterizes the weathering products formed from leaching of basalt and adds in a detailed analysis of the remotely sensed signatures.

## 3. Sampling Site

[9] Samples were collected along a vertical profile of altered Deccan basalts in Bidar, India, near Hyderabad, at 17°54′58.8″N, 77°32′34.3″E. The basalts at this site have undergone different degrees of leaching to form saprolite and laterite units that can be investigated further using spectroscopic and laboratory analyses to better understand phyllosilicate mineral occurrences and their assemblages on Mars. Saprolites form through isovolumetric weathering where pseudomorphic replacement of the primary minerals preserves the fabric and textures of the original basalt [e.g., *Merino et al.*, 1993]. A bole horizon forms when the top of one lava flow is altered and then a second flow caps the first, preserving the altered section below it [*Widdowson et al.*, 1997]. The saprolite here is preserved as a bole horizon that has recently been exposed in a quarry. While the saprolite is thicker than a typical bole horizon, thicker weathering profiles with unaltered basalt at the base and progressively more altered material upward are sometimes preserved in the Deccan traps as bole horizons [*Nesbitt and Wilson*, 1992; *Widdowson et al.*, 1997]. The exact definition of laterite is debated, but laterites are extremely leached horizons enriched in Al and Fe oxides and oxyhydroxides and kaolinite [*Bourman and Ollier*, 2002; *Schellmann*, 1981].

[10] The stratigraphy and sampling locations at this vertical section are shown in Figure 1. Unaltered basalt at the base of this vertical section grades into a thick saprolite. Rims of corestones are visible lower in the saprolite, but the interiors have been completely altered in the main section. A mottled zone is found higher in the sequence. The saprolite is capped by a second basalt layer. Samples HYD-5 to 12 were collected in a quarry that exposes the saprolite and overlying basalt. HYD-4 was collected in a creek bed near the quarry and is a sample of the basalt at the base of the saprolite. HYD-3 was collected partway up a hill adjacent to the quarry and is part of the saprolite, but its exact stratigraphic location with respect to the other saprolite samples is unclear. HYD-13 was taken from a laterite at the top of the hill that lies stratigraphically above the second layer of basalt. Samples HYD-0 to 2 are from a nearby quarry at 17°54′48.3″N, 77°32′47.5″E. Their stratigraphic placement in the vertical section is unknown, but similarities of these samples to those in the vertical section can help confirm relationships between different types of samples. Although the traditional sequence from basalt to saprolite to laterite typically seen in weathering profiles has been broken up in this section, all of the components are represented and can still be studied to understand the differences in mineralogy, chemistry, and spectroscopic signatures as basalts are leached to smectite and then kaolinite.

[11] Samples HYD-0, HYD-4, HYD-5, and HYD-11 are crystalline, igneous basalt. HYD-4, HYD-5, and HYD-11 are from the vertical section (Figure 1), while HYD-0 was collected nearby. All except HYD-0 have weathering rinds ranging from one less developed and slightly darker than the interior (HYD-11) to a thin brown and black rind (HYD-4) to an extensive coating of red, yellow, and brown secondary minerals (HYD-5). The saprolite samples are HYD-3, HYD-6, HYD-8, HYD-9, and HYD-10, and all but HYD-3 are from the vertical section. Colors range from gray to brown and black. All samples are soft and friable and visually consist mostly of clays, but there are occasional larger crystals of zeolites. HYD-3 and HYD-10, from the base of the saprolite, contain zeolites throughout the samples. HYD-8 and HYD-9 were taken from a mottled zone higher, with HYD-9 in the redder, more oxidized zone and HYD-8 in the grayer, less oxidized portion, and HYD-6 is from the top of the saprolite just below the second layer of basalt. The samples HYD-7 and HYD-12 are both zeolites that likely precipitated in fractures in the original basalt rock. HYD-12 is from the base of the saprolite near HYD-10 and has larger, whiter, transparent crystals. Some of the crystals are more blocky and rectangular, while other crystals are more similar in appearance to HYD-7. HYD-7, from the top of the saprolite near HYD-6, has large, fan-shaped, semitransparent crystals that seem to be coated in fine, red dust. HYD-7 appears to have a more uniform mineralogy while HYD-12 visibly seems to have a mixture of different zeolite minerals. HYD-13 is a

laterite sample that caps this vertical section, and HYD-1 and HYD-2 were collected from nearby laterites. Samples HYD-2 and HYD-13 are reddish-brown, and HYD-1 has a grayer interior with a red-brown weathering rind. These samples are soft but better cemented than some of the saprolite samples.

[12] Basalts near Bidar, where the vertical section is located, have been identified to be part of the Ambenali Formation in the Wai Sub-Group [*Jay and Widdowson*, 2008]. Previous work has been done on a weathering profile in Bidar that contains unaltered basalt at the base up through a laterite cap [*Kısakürek et al.*, 2004; *Wimpenny et al.*, 2007]. Enrichments and depletions of Fe, which is sensitive to redox conditions, and mobile elements show that this profile from the base through the saprolite was below a paleo-water table, and Li isotopes show that the profile received aeolian input [*Kısakürek et al.*, 2004]. The sequence has also been found to be enriched in Os, which may result from a combination of aeolian input and lateral transport by groundwater [*Wimpenny et al.*, 2007]. The vertical section studied in this paper is different from the one investigated by *Kısakürek et al.* [2004] and *Wimpenny et al.* [2007] but has likely been similarly affected by the paleo-water table and aeolian input.

## 4. Methods

### 4.1. Visible and Near Infrared Spectroscopy and Mid-infrared Spectroscopy

[13] Bulk samples were first characterized with an Analytical Spectral Devices (ASD) spectrometer from 0.35 to 2.5 $\mu$m. Both interiors and exteriors were measured on rock samples with a weathering rind or coating. Each sample was then ground with a mortar and pestle, and an effort was made to only grind the interiors of the samples. Ground samples were dry-sieved into <45, 45–125, 125–500, and >500 $\mu$m separates. The size ranges of the separates were optimized for visible and near infrared spectroscopy. All separates were measured with the ASD. The 45–125 $\mu$m separates were measured in the Keck/NASA Reflectance Experiment Laboratory (RELAB) by the bidirectional spectrometer from 0.28 to 2.6 $\mu$m and by the Fourier Transform Infrared (FTIR) spectrometer in an $H_2O$ and $CO_2$ purged environment from 0.7999 to 25.0502 $\mu$m [*Pieters*, 1983]. Kirchhoff's law, $\varepsilon = 1 - R$, relating reflectance ($R$) and emissivity ($\varepsilon$) can be used to approximate emissivity from reflectance measurements [*Mustard and Hays*, 1997; *Salisbury et al.*, 1994]. Although samples were measured in units of reflectance, mid-IR reflectance spectra were converted to emissivity with Kirchhoff's law and are shown in units of (1 – Reflectance), or emissivity. Spectra in the visible and near infrared are shown in units of wavelength ($\mu$m), while spectra in the mid-IR are shown in wavenumber ($cm^{-1}$) to conform to convention.

### 4.2. X-Ray Diffraction

[14] X-ray diffraction (XRD) analyses were done at the United States Geological Survey (USGS) to identify crystalline phases in each sample. Powdered XRD scans were collected on a PANalytical 'X'Pert Pro – MPD X-ray Diffractometer. The scan range was 5–65 degrees two-theta, sample spinner on, and the scan rate was 0.167 degree per minute for a total scan time of six hours per sample. Mineral identifications were made using MDI Whole Pattern Fit software which calculates a whole pattern fit and a Rietveld refinement of the minerals [*Young*, 1995]. Additional analyses were done on the clay fraction of HYD-9. That sample was sonified and then settled in a 1000 ml graduated cylinder for 30 minutes. The top 200 ml were collected to isolate material less than 8 $\mu$m. Oriented clay mounts were scanned following USGS clay identification procedures. There were four scans under the following conditions: air dried, ethylene glycolated, heat treated (400°C for 1 hour), and heat treated (500°C for 1 hour).

### 4.3. Major Element Chemistry and Loss on Ignition

[15] Concentrations of ten major elements (Al, Ca, Fe, K, Mg, Mn, Na, P, Si, Ti) were determined with an inductively coupled plasma atomic emission spectrometer (ICP-AES) after a flux fusion sample preparation following the methods of *Murray et al.* [2000]. This method was selected because it measures the bulk composition of the samples and does not have biases common to other methods such as scanning electron microscopy that measure composition of very small areas. For each ground sample, 40 $\pm$ 5 mg was mixed with 150 $\pm$ 5 mg lithium metaborate flux in graphite crucibles. Six standard reference materials (BCR-2, BHVO-2, SGR-1, Mag-1, NIST2711, and NIST1646a) and three blanks with only lithium metaborate were prepared in the same manner. Two unknown samples were run in duplicate, and one was run in triplicate. The samples, blanks, and standards were fused with the flux in a 1050°C oven for 10 min, immediately poured into 20 ml 10% nitric acid, and agitated for at least 30 min. They were then filtered with a 0.45-$\mu$m Gelman filter and diluted further. Before running the samples on the ICP-AES, liquid standards were made with varying amounts of each major element and then measured by the ICP-AES. The samples, blanks, and flux fusion standards were run in a random order on the ICP-AES, and elemental concentrations were determined using the intensities of peaks at wavelengths suggested by *Murray et al.* [2000]. The measurements were corrected for drift and blanks were subtracted. Linear regressions from the standards were used to correct elemental abundances in the unknown samples for losses during the flux fusion process. In keeping with geochemical convention, data are reported in wt % oxide. Approximately 1 g of each sample was heated at 550°C for four hours and then cooled overnight in a desiccator. The difference in mass before and after heating was the loss on ignition (LOI).

### 4.4. Mössbauer Spectroscopy

[16] Mössbauer spectra were acquired at Mount Holyoke College of all samples except HYD-7 and HYD-12, which had too little Fe, and calibrated relative to the spectrum of a 25-$\mu$m Fe foil. The Mexdisd and Mexfield programs designed by Eddy De Grave and Toon Van Alboom at the University of Ghent were used to model the spectra using the methods of *Vandenberghe et al.* [1994]. Both Mexdisd and Mexfield solve the full hyperfine-interaction Hamiltonian using center shift, quadrupole shift, and line width as adjustable parameters to optimize the fit in the chi-square sense [*Vandenberghe et al.*, 1994]. The programs differ in that Mexdisd creates a probability distribution of hyperfine field values, whereas Mexfield finds a single value, so the

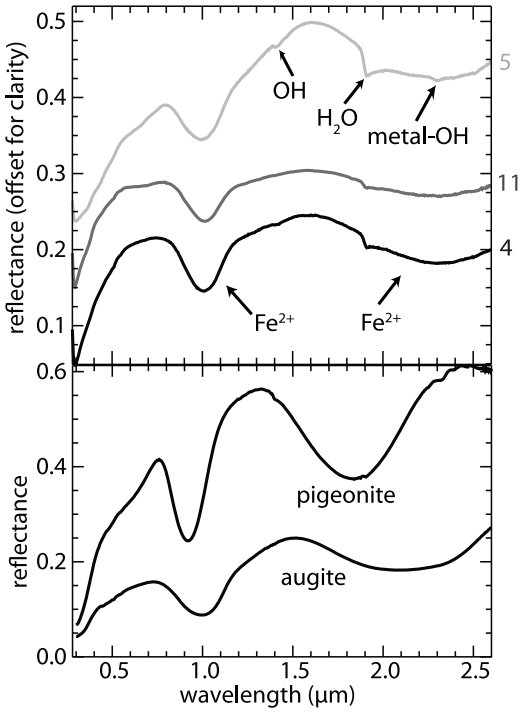


**Figure 2.** (top) Bidirectional reflectance spectra acquired in RELAB of basalt samples HYD-4 (4), HYD-11 (11), and HYD-5 (5). The VNIR spectrum of HYD-11 has been multiplied by 2 to increase the contrast. (bottom) Library spectra of augite (C1PP49) and pigeonite (C1PP42) for reference [*Murchie et al.*, 2007].

programs can produce different line shapes. Mexfield is preferential in highly overlapped or low resolution spectra. Errors on results for well-resolved components are usually ca. 0.02–0.04 mm/s for isomer shifts, quadrupole splitting and linewidths, ~0.1–0.3 Tesla for magnetic hyperfine fields, and 1–3% (absolute) for relative areas of distributions.

## 5. Results

### 5.1. VNIR Spectroscopy

[17] At the shortest wavelengths (<~1 $\mu$m), spectra may have broad crystal field and charge transfer absorptions from transition metals such as Fe [*Burns*, 1993; *Scheinost et al.*, 1998]. Shifts in the center wavelength and shape of these features are indicative of the presence of various Fe-bearing minerals such as olivine, pyroxene, and Fe-oxides [e.g., *Cloutis and Gaffey*, 1991; *Scheinost et al.*, 1998]. In pyroxenes, there is a second crystal field absorption near 2.0 $\mu$m due to $Fe^{2+}$, which is at a slightly shorter wavelength in low-Ca pyroxene and a slightly longer wavelength in high-Ca pyroxene [*Adams*, 1974; *Burns*, 1993; *Cloutis and Gaffey*, 1991].

[18] Vibrational absorption features in the near infrared are overtones and combination tones related to $H_2O$ and OH [*Clark et al.*, 1990]. The exact wavelength of the minimum in this region and the number of minima is related to the structure and coordination of -OH by cations [e.g., *Bishop et al.*, 2008b]. Absorptions at 1.4 $\mu$m are the first OH stretching overtone, and absorptions at 1.9 $\mu$m are a combination tone of the H-O-H bend and OH stretch [*Clark et al.*, 1990]. In some minerals such as zeolites, additional overtones and combination tones can also be seen near 0.97 $\mu$m (second overtone of the $H_2O$ stretch) and 1.161 $\mu$m (bend and symmetric and asymmetric stretch of bound $H_2O$) [*Cloutis et al.*, 2002]. Metal-OH combination bands occur from 2.20 to 2.35 $\mu$m and shift depending on the metal [*Clark et al.*, 1990]. In smectite, these absorption features occur near 2.20 $\mu$m from $Al_2$-OH bonds, 2.24–2.26 $\mu$m from $AlFe^{3+}$-OH, 2.29 $\mu$m from $Fe^{3+}$-OH, and 2.30–2.34 $\mu$m from Mg-OH [*Andrieux and Petit*, 2010; *Bishop et al.*, 2008b; *Clark et al.*, 1990]. The presence of an absorption feature at 1.9 $\mu$m from structural $H_2O$ with a metal-OH combination band is diagnostic of smectite clays [e.g., *Bishop et al.*, 2002a; *Clark et al.*, 1990]. The exact position of the metal-OH feature can distinguish different smectites [*Clark et al.*, 1990]. Doublets or triplets near 1.4 and 2.2 $\mu$m are characteristic of kaolin group minerals such as kaolinite and halloysite [*Clark et al.*, 1990]. The exact wavelength of the fundamental OH stretching vibration at 2.67–2.94 $\mu$m depends on the particular cations (e.g., Al, Mg, Fe) coordinated by OH and the crystal structure and shifts with different mineralogies and compositions [e.g., *Bishop et al.*, 2008b; *Farmer*, 1974]. In smectite clays, a fundamental vibrational absorption feature from $Al_2OH$ stretching occurs at 2.75–2.76 $\mu$m, which can be difficult to distinguish from the MgAlOH stretching vibration at 2.71 $\mu$m [*Farmer*, 1974]. Absorption features from $Mg_3OH$ fundamental stretching vibrations occur at shorter wavelengths (~2.69–2.72 $\mu$m) [*Farmer*, 1974]. If $Fe^{3+}$ is present in the structure, the fundamental OH stretching vibrations are broader and occur at longer wavelengths [*Farmer*, 1974]. The fundamental $H_2O$ bending vibration occurs at 6.0–6.2 $\mu$m [*Bishop et al.*, 2008b].

[19] The position, strength, and shape of absorption features in VNIR spectra of HYD-0, HYD-4, HYD-5, and HYD-11 are all consistent with basalt (spectra of HYD-4, HYD-5, and HYD-11 and library spectra are shown in Figure 2). All have broad absorption features centered at 1.00–1.03 and 2.20–2.30 $\mu$m due to crystal field transitions of $Fe^{2+}$ [*Burns*, 1993; *Cloutis and Gaffey*, 1991]. These band centers are consistent with the presence of high-Ca pyroxene in the samples [*Burns*, 1993; *Cloutis and Gaffey*, 1991]. While the features from crystal field transitions are similar among all of these samples, they have differences in vibrational absorption features indicative of hydration and alteration. HYD-0, which is not from the profile, and HYD-11 have weak H-O-H bend and OH stretch combination tones at 1.91 $\mu$m and poorly defined fundamental OH stretching vibrations at 2.7–2.9 $\mu$m, suggesting that the samples have a small amount of a hydrated phase [*Bishop et al.*, 2008b; *Clark et al.*, 1990; *Farmer*, 1974]. These absorption features are not diagnostic of any particular hydrated mineral. HYD-4 and HYD-5 have overtones and combination tones of OH and $H_2O$ at 1.4 and 1.9 $\mu$m [*Clark et al.*, 1990] and deeper absorptions at 2.70–2.80 $\mu$m, suggesting that these samples are more altered than HYD-0 and HYD-11. The 2.71, 2.76, and 2.80 $\mu$m fundamental OH stretching vibrations in HYD-4 suggest the presence of Fe-smectite or chlorite and possibly chamosite, glauconite, or an Al-rich dioctahedral mica [*Bishop et al.*, 2008b; *Farmer*, 1974]. In HYD-5, the crystal field transition centered at 2.20–2.30 $\mu$m is less well-expressed than in

other samples and is modified by the presence of overtones and combination tones of hydrated minerals at 1.91 and 2.30 $\mu$m. Taken with a fundamental OH vibration at 2.80 $\mu$m, this sample probably contains some Fe/Mg-smectite or chlorite [*Bishop et al.*, 2008b; *Clark et al.*, 1990; *Farmer*, 1974].

[20] Moving upward in an idealized weathering stratigraphy, VNIR spectra of samples from the saprolite, HYD-3, HYD-6, HYD-8, HYD-9, and HYD-10 (Figure 3a), retain none of the mafic signatures of the original basalts and are completely dominated by overtones and combination tones of hydrous minerals, despite XRD and Mössbauer analyses that show the presence of mafic minerals in some samples. Spectra of all samples have both an H-O-H bend and OH stretch at 1.9 $\mu$m and a metal-OH combination band at 2.20–2.35 $\mu$m, indicating that they contain various smectite clays [*Bishop et al.*, 2008b; *Clark et al.*, 1990]. Other features present in all spectra include charge transfers at wavelengths less than approximately 0.8 $\mu$m that control the shape of the spectra [*Burns*, 1981; *Sherman and Waite*, 1985], an OH stretching overtone near 1.4 $\mu$m, and a deep fundamental OH stretching vibration at 2.7–2.8 $\mu$m [*Bishop et al.*, 1994; *Clark et al.*, 1990; *Farmer*, 1974]. Variations in the presence or position of absorption features in different samples are indicative of differences in mineralogy and chemistry. HYD-3 shows a crystal field transition centered at 0.90–0.95 $\mu$m consistent with $Fe^{3+}$ [*Scheinost et al.*, 1998]. In ASD spectra of the largest separates and the unground sample, overtones and combination tones of $H_2O$ near 0.98 and 1.16 $\mu$m are present from zeolites in the sample [*Cloutis et al.*, 2002], but these features are not seen in smaller separates as the spectra become dominated by smectite clays. Exact positions of absorption features for HYD-3 at 1.425, 2.21 (very weak), 2.25 (weak), 2.30, and 2.79 $\mu$m all suggest a predominantly $Fe^{3+}$-bearing phyllosilicate such as nontronite or chlorite. HYD-10, at the base of the section, has the same overtones and combination tones as HYD-3 from zeolites at wavelengths less than 1.2 $\mu$m in spectra of larger separates. HYD-10 also shows a weak crystal field transition centered at 1.0–1.1 $\mu$m from Fe-oxide [*Scheinost et al.*, 1998]. Absorption features at 1.42, 2.21 (weaker), 2.30, and 2.79 $\mu$m are all consistent with a mostly $Fe^{3+}$-bearing smectite but with some Al-rich smectite [*Bishop et al.*, 2008b; *Clark et al.*, 1990]. The depths of 1.4 and 1.9 $\mu$m features in HYD-3 and HYD-10 are probably enhanced because of the overlapping absorptions of $H_2O$ in the zeolites. Moving up in the section, HYD-8 has absorption features at 1.42, 2.21, 2.24, 2.29, 2.76, and 2.80 $\mu$m and probably has a mixture of both Al- and Fe-bearing smectite clays, such as montmorillonite and nontronite or possibly chlorite [*Bishop et al.*, 2008b; *Clark et al.*, 1990]. HYD-9, which is mottled with HYD-8, has a mixture of Al-, Fe-, and Mg-bearing smectite clays, based on the presence of features at 1.41, 2.21, 2.25, 2.295, and 2.75 $\mu$m [*Bishop et al.*, 2008b; *Clark et al.*, 1990]. HYD-9 also has a weak crystal field transition centered at 1.0–1.1 $\mu$m either from Fe-oxide or $Fe^{3+}$ in nontronite [*Bishop et al.*, 2008b; *Burns*, 1993; *Scheinost et al.*, 1998]. Finally, HYD-6, at the top of the section, has absorption features at the same wavelengths as HYD-8, although the absorption features in HYD-6 are generally sharper, with an additional feature at 2.705 $\mu$m and are consistent with similar Al- and Fe-bearing smectite clays to HYD-8 [*Bishop et al.*, 2008b; *Clark et al.*, 1990]. In all spectra, shifts in the position and broadening of the 1.4 $\mu$m OH stretching overtone (Figure 3b), multiple absorption features from metal-OH combination bands at 2.20–2.35 $\mu$m (Figure 3c), and fundamental OH stretching vibrations at 2.70–2.80 $\mu$m (Figure 3d) all indicate the complex nature of the clays in these samples [*Bishop et al.*, 1994; *Clark et al.*, 1990; *Farmer*, 1974]. These samples may be interlayered illite/smectite, or smectite with other minerals, but it is difficult to determine if these are mixed layered clays with spectroscopy. The presence of mixed layered clays could account for asymmetries in absorption features or complexities in the spectra [e.g., *Milliken and Bish*, 2010; *Milliken et al.*, 2010].

[21] There are zeolites throughout the saprolite, and two samples (HYD-7 and HYD-12) of nearly pure zeolites were analyzed. VNIR spectra of these samples (Figure 4) are dominated by features related to bound and adsorbed water in the zeolite structure. The spectra are relatively featureless below approximately 900 nm due to the absence of Fe or other transition metals in the samples. Spectra in the infrared are dominated by overtones, combination tones, and fundamental vibrations of $H_2O$ and OH in the zeolites: 0.97–0.975 $\mu$m (second $H_2O$ stretching overtone), 1.161 $\mu$m in HYD-7 and 1.164 $\mu$m in HYD-12 (bend and stretch combination of bound $H_2O$), 1.426 $\mu$m in HYD-7 and 1.431 $\mu$m in HYD-12 (bound $H_2O$ combination), 1.468 $\mu$m (adsorbed $H_2O$ combination), $\sim$1.92 $\mu$m ($H_2O$ stretch and bend combination), and 2.769 $\mu$m in HYD-7 and $\sim$2.79 $\mu$m in HYD-12 ($H_2O$ stretch) [*Cloutis et al.*, 2002]. The exact minima of different absorption features are indicative of the chemistries of the samples [*Cloutis et al.*, 2002]. Both samples are consistent with Ca-rich zeolites, and HYD-12 has more Ca relative to Na than HYD-7 [*Cloutis et al.*, 2002]. VNIR spectra of both are consistent with chabazite and stilbite spectra in the CRISM and USGS spectral libraries [*Clark et al.*, 2007; *Murchie et al.*, 2007].

[22] HYD-1, HYD-2, and HYD-13 are samples of laterites. VNIR spectra of these samples all show a mixture of kaolin group minerals and Fe-oxides (the spectrum of HYD-13 is shown in Figure 5a). The samples all have broad absorption features at wavelengths less than 1.0 $\mu$m from crystal field transitions of Fe in various Fe-oxides and sharper absorption features diagnostic of kaolin group minerals in the infrared (doublets near 1.4 and 2.2 $\mu$m from $Al_2OH$ overtones and combination tones and a series of features near 2.7–2.8 $\mu$m from the fundamental OH vibrations of the inner and outer OH groups) [e.g., *Bishop et al.*, 2008b; *Clark et al.*, 1990; *Farmer*, 1974]. None of the samples show a triplet near 1.4 $\mu$m diagnostic of well-crystalline kaolinite, so the samples contain either poorly crystalline kaolinite or halloysite [*Clark et al.*, 1990]. These spectra also all have 1.9 $\mu$m absorption features from the H-O-H combination bend and stretch of structural $H_2O$ [e.g., *Bishop et al.*, 2008b; *Clark et al.*, 1990]. Kaolinite does not have structural water, but halloysite does [*Clark et al.*, 1990]. This 1.9 $\mu$m feature may provide additional evidence that these samples, particularly HYD-13, contain halloysite. Alternatively, there may be some interlayered smectite in the samples, there may be adsorbed $H_2O$, or the samples may simply be wet, despite being dried overnight in a desiccator. There is some variation in spectra of different laterite samples indicative of differences in the exact kaolin group mineral or Fe-oxide present in each sample. The approximate positions of the crystal field transitions at 520–550 nm and 900 nm in HYD-1 and HYD-13

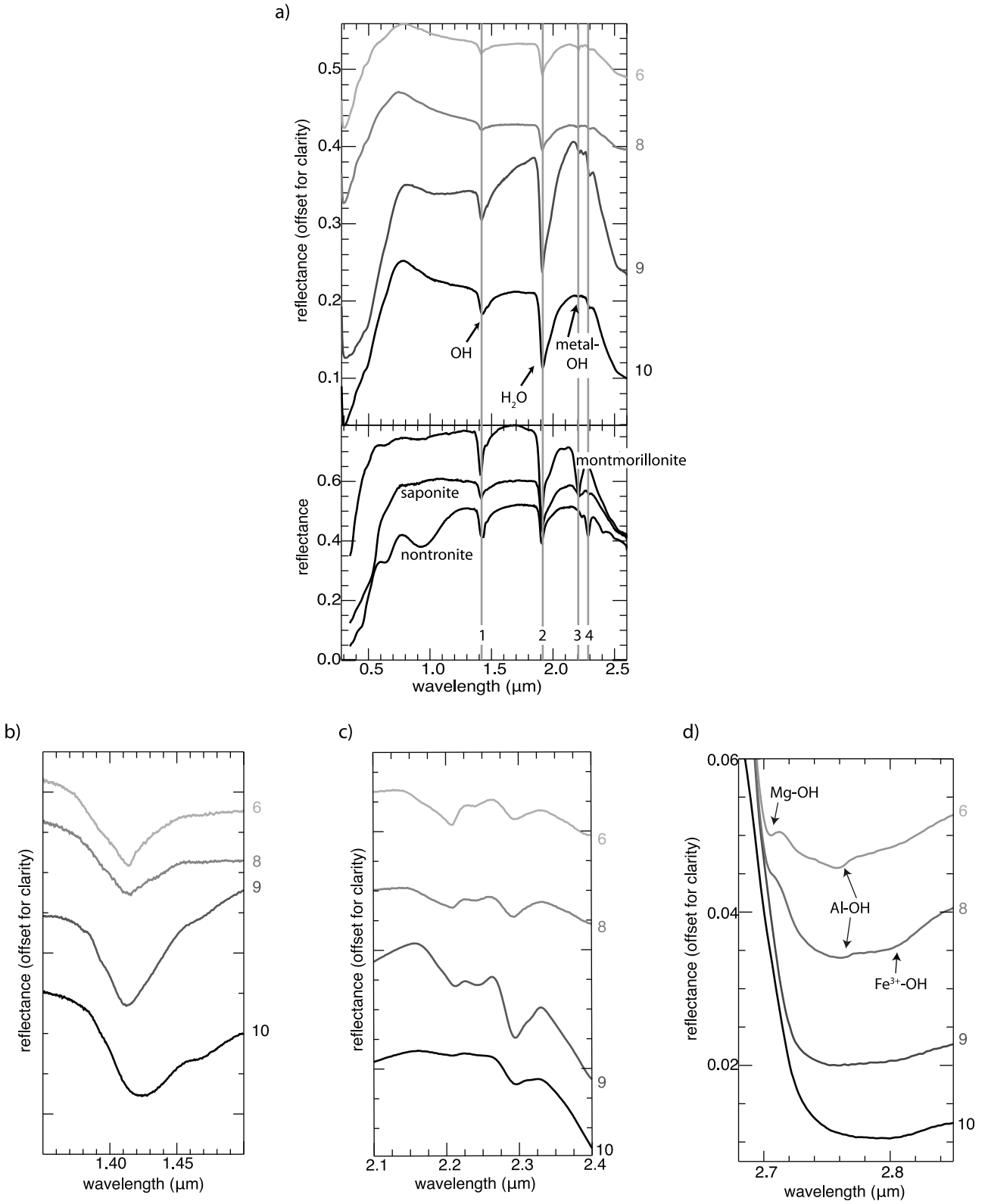


**Figure 3.** (a) Bidirectional reflectance spectra in the (top) VNIR of saprolite samples acquired in RELAB and (bottom) library spectra of montmorillonite (CAMO02), saponite (LASA57), and nontronite (CCJB26) for reference [*Murchie et al.*, 2007]. Lines at 1.41 (1), 1.91 (2), 2.20 (3), and 2.29 $\mu$m (4) are shown for visual guidance. (b) Close-up of the first OH stretching overtone near 1.4 $\mu$m (FTIR spectra), (c) 2.2–2.35 $\mu$m metal-OH combination bands (FTIR spectra), and (d) fundamental OH stretching vibration region (FTIR spectra). Spectra shown are HYD-6 (6), HYD-8 (8), HYD-9 (9), and HYD-10 (10). Spectra of HYD-6 and HYD-8 in Figures 3b and 3d have been multiplied by 2 to increase contrast.

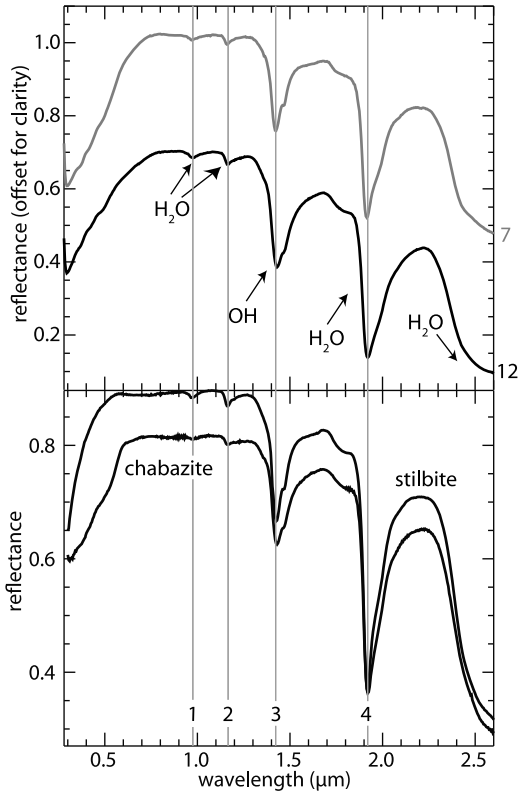


**Figure 4.** (top) RELAB bidirectional reflectance spectra of pure zeolite samples HYD-7 (7) and HYD-12 (12) in the VNIR and (bottom) library spectra of chabazite (C1ZE18) and stilbite (C1ZE21) [*Murchie et al.*, 2007]. Lines at approximately 0.97 (1), 1.16 (2), 1.141 (3), and 1.91 $\mu$m (4) are shown for visual guidance.

are consistent with hematite in the samples, while the center wavelengths around 490 and 980 nm for HYD-2 suggest goethite [*Scheinost et al.*, 1998]. The wavelengths of doublets in spectra of HYD-1 and HYD-2 at 1.395 and 1.415 $\mu$m and 2.165 and 2.209 $\mu$m suggest that these samples are kaolinite with poorer crystallinity [*Clark et al.*, 1990]. Additional absorption features in HYD-1 and HYD-2 at 2.24 $\mu$m and 2.78 $\mu$m may indicate that there is some Fe-bearing montmorillonite or another Fe- and Al-bearing clay in these samples [*Bishop et al.*, 2008b; *Clark et al.*, 1990]. Fundamental vibrational absorption features occur at 2.71, 2.725, and 2.74 $\mu$m from inner OH group stretching vibrations and 2.76 $\mu$m from outer OH group stretching vibrations of kaolinite in both HYD-1 and HYD-2 [*Bishop et al.*, 2008b; *Farmer*, 1974]. The spectrum of HYD-13 has doublets at 1.389 and 1.414 $\mu$m and 2.182 and 2.208 $\mu$m is more consistent with halloysite [*Clark et al.*, 1990]. Fundamental OH vibrations occur at 2.705, ~2.738, and 2.760 $\mu$m in HYD-13 (Figure 5b) are also consistent with a kaolin group mineral [*Bishop et al.*, 2008b].

### 5.2. Mid-IR Spectroscopy

[23] In the mid-IR, the Christiansen feature is a maximum in emissivity and occurs at 1333–1111 cm$^{-1}$ (7.5–9 $\mu$m) as the real index of refraction passes through 1.0 [*Salisbury and Walter*, 1989]. Its frequency reflects the composition and degree of Si-O bonding in the sample: those with low Fe and a high degree of Si-O bonding will have a Christiansen feature at the longest wavenumbers (shortest wavelengths), while samples with high Fe and few Si-O bonds will have a Christiansen feature at the shortest wavenumbers (longest wavelengths) [*Salisbury and Walter*, 1989]. In zeolites, the Christiansen feature position depends on the Al:(Al + Si) ratio [*Cloutis et al.*, 2002]. Reststrahlen bands, which are Si-O stretching vibrations, occur at wavenumbers shorter than the Christiansen feature to ~800 cm$^{-1}$ (12.5 $\mu$m) [e.g., *Hamilton*, 2000; *Nash and Salisbury*, 1991; *Strens*, 1974].

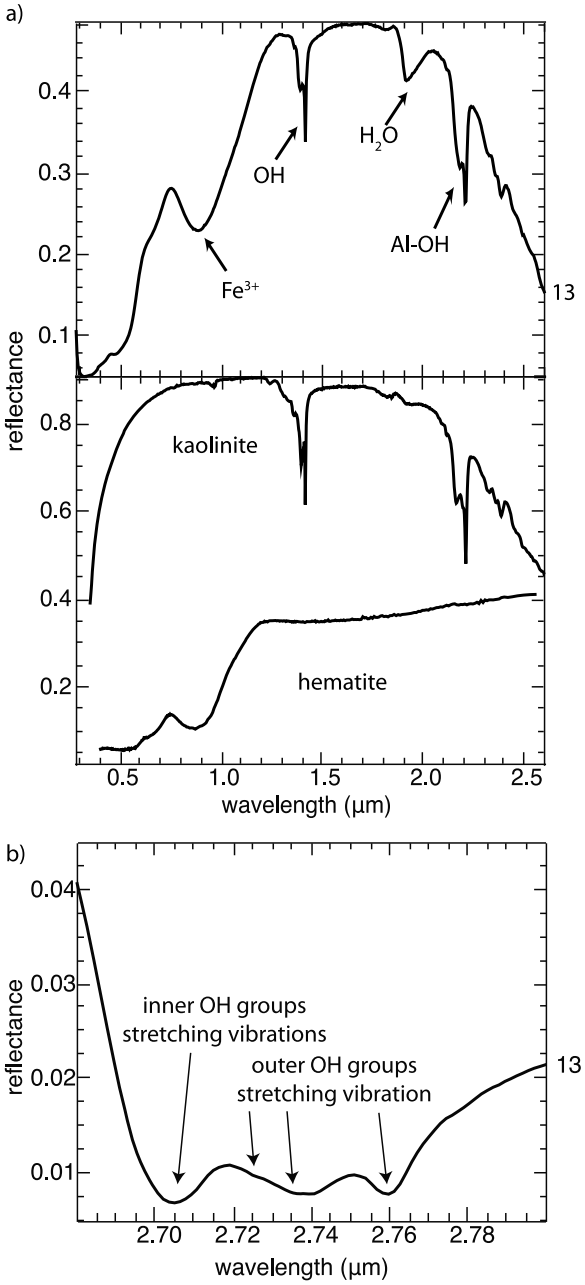


**Figure 5.** Spectra of laterite sample in (a) VNIR (top; bidirectional reflectance spectra from RELAB) with (bottom) library spectra of kaolinite (CDJB25) and hematite (Fe2602) [*Clark et al.*, 2007; *Murchie et al.*, 2007] and (b) fundamental OH stretching region (FTIR spectra from RELAB).

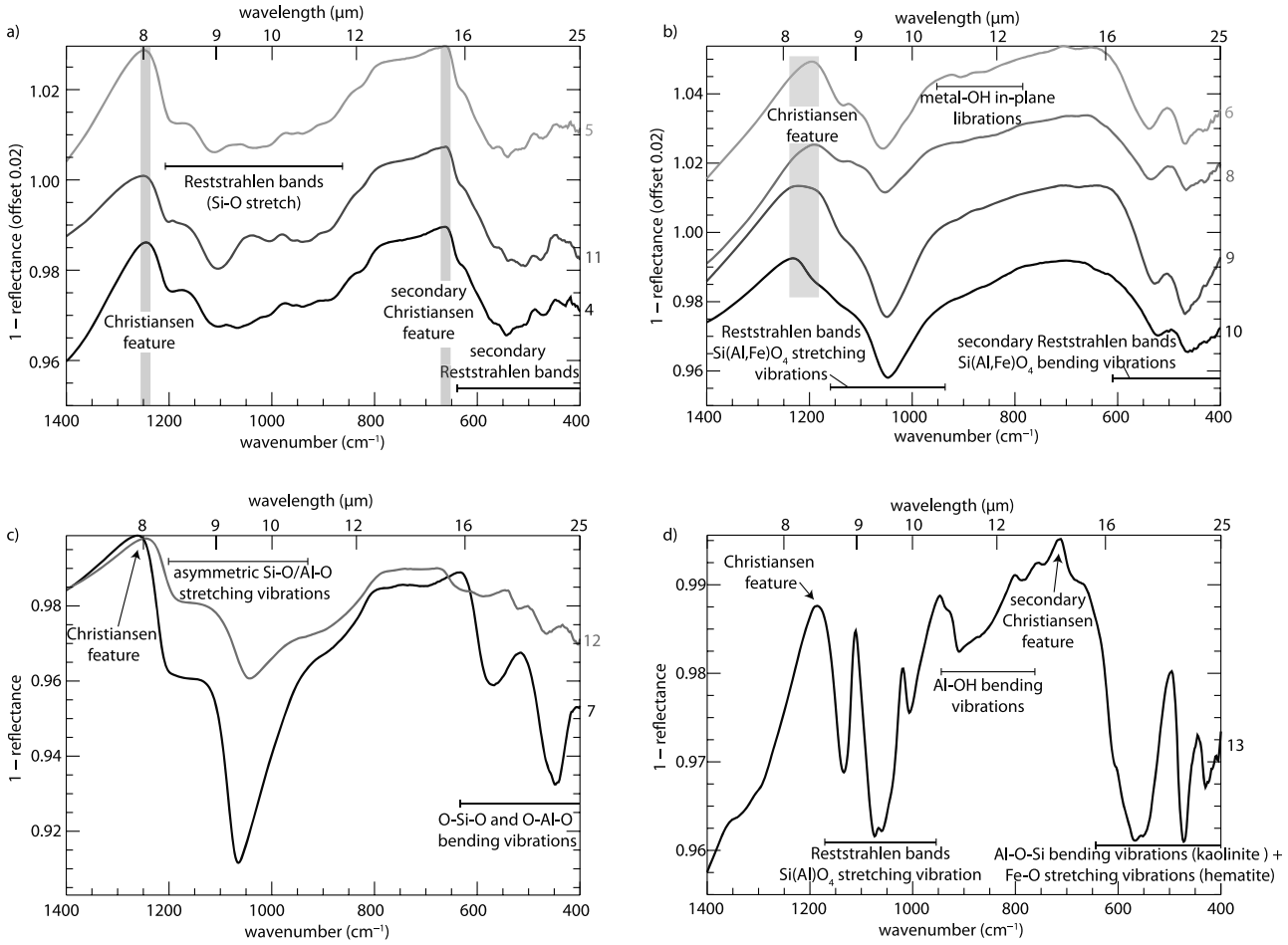


**Figure 6.** (a) Mid-IR spectra of basalt samples HYD-4 (4), HYD-11 (11) and HYD-5 (5), (b) saprolite samples HYD-6 (6), HYD-8 (8), HYD-9 (9), and HYD-10 (10), (c) zeolite samples HYD-7 (7) and HYD-12 (12), and (d) laterite sample HYD-13 (13). All spectra are FTIR spectra from RELAB.

The shape and center wavelengths of these vibrations are characteristic of mineralogy and bonding and are the convolution of the absorptions from multiple minerals [e.g., *Feely and Christensen*, 1999; *Wyatt et al.*, 2001]. Substitutions of Fe and Al for Si in tetrahedra affect the position of the Reststrahlen bands of phyllosilicate minerals [*Bishop et al.*, 2002a, 2008b; *Farmer*, 1974; *Michalski et al.*, 2006]. Metal-OH bending vibrations occur at 950–590 $cm^{-1}$ (11–17 $\mu$m) in phyllosilicates [e.g., *Bishop et al.*, 2008b; *Michalski et al.*, 2005]. At small grain sizes, transparency features can be seen from 833 to 625 $cm^{-1}$ (12–16 $\mu$m). Secondary Reststrahlen bands occur at 600–400 $cm^{-1}$ (16.7–25 $\mu$m) due to Si-O-Si bending vibrations [e.g., *Hamilton*, 2000]. These features are near 556–400 $cm^{-1}$ (18–25 $\mu$m) in phyllosilicate minerals [*Bishop et al.*, 2008b; *Michalski et al.*, 2005].

[24] Mid-IR spectra of HYD-4, HYD-5, and HYD-11 are shown in Figure 6a. The Christiansen frequencies of these spectra and HYD-0 range from 1250 to 1240 $cm^{-1}$ (8.0–8.06 $\mu$m) and are in the range expected for mafic compositions [*Salisbury and Walter*, 1989; *Wyatt et al.*, 2001]. The narrow range in position of this feature across these samples is consistent with their low chemical and mineralogical diversity. Reststrahlen bands occur in these samples from 1220 to 850 $cm^{-1}$ (8.2–11.8 $\mu$m) from Si-O stretching vibrations of minerals such as pyroxene and plagioclase [*Hamilton*, 2000; *Nash and Salisbury*, 1991]. The shape of these bands is consistent with reported basalt spectra and results from the convolution of absorptions from plagioclase, pyroxene, and other minerals [*Feely and Christensen*, 1999; *Wyatt et al.*, 2001]. Another complex set of absorption features can be seen from 600 to 400 $cm^{-1}$ (16.7–25 $\mu$m) from Si-O-Si bending vibrations, lattice modes, and stretching vibrations of metal cation-oxygen bonds [*Hamilton*, 2000].

[25] Spectra of the saprolite samples HYD-3, HYD-6, HYD-8, HYD-9, and HYD-10 (Figure 6b shows all but HYD-3) generally are consistent across samples. All spectra indicate that the samples are smectite-bearing, with Christiansen features from 1230 to 1170 $cm^{-1}$ (8.13 to 8.55 $\mu$m), Reststrahlen bands at 1100–1000 $cm^{-1}$ (9.1–10 $\mu$m), and doublets at 400–600 $cm^{-1}$ (16.7–25 $\mu$m). The Christiansen feature positions are modified by the presence of pyroxene and/or zeolites in the samples, which should shift the Christiansen features to shorter and longer wavenumbers, respectively [*Salisbury and Walter*, 1989]. The position of the Reststrahlen bands are related to the Al and Fe substitution for Si in tetrahedra and the specific cations involved in

**Table 1.** Major Element Chemistry Results From ICP-AES and Presence/Absence of Minerals From XRD in All Samples

| Sample | Type | $Al_2O_3$ | CaO | $Fe_2O_3$ | $K_2O$ | MgO | MnO | $Na_2O$ | $P_2O_5$ | $SiO_2$ | $TiO_2$ | LOI | Px[a] | Plag[b] | Phyllo[c] | Zeolite | Fe/Ti-Oxides |
|---|---|---|---|---|---|---|---|---|---|---|---|---|---|---|---|---|---|
| *Samples From Vertical Section (in Stratigraphic Order)* | | | | | | | | | | | | | | | | | |
| HYD-13 | Laterite | 30.03 | 0.04 | 19.35 | 0.20 | 0.10 | 0.13 | 0.03 | 0.05 | 34.11 | 2.32 | 12.66 | | | X | | X |
| HYD-5 | Basalt | 14.75 | 10.44 | 12.98 | 0.25 | 6.45 | 0.16 | 2.50 | 0.21 | 48.69 | 2.16 | 2.19 | X | X | X | | X |
| HYD-11 | Basalt | 14.23 | 10.30 | 12.59 | 0.19 | 6.26 | 0.19 | 2.38 | 0.20 | 48.26 | 2.23 | 0.75 | X | X | X | | X |
| HYD-6 | Saprolite | 14.78 | 1.95 | 12.55 | 0.19 | 3.69 | 0.13 | 0.16 | 0.21 | 36.16 | 2.75 | 17.56 | | | X | | X |
| HYD-7 | Zeolite | 16.58 | 7.17 | 1.85 | 0.04 | 0.76 | 0.02 | 0.88 | 0.02 | 56.60 | 0.23 | 17.91 | | | | X | |
| HYD-8 | Saprolite | 16.90 | 4.30 | 15.20 | 0.25 | 2.98 | 0.21 | 1.26 | 0.29 | 44.80 | 3.21 | 13.88 | X | X | X | | X |
| HYD-9 | Saprolite | 11.27 | 2.41 | 12.95 | 0.19 | 6.04 | 0.13 | 0.09 | 0.03 | 41.23 | 3.12 | 19.17 | | | X | | X |
| HYD-10 | Saprolite | 13.37 | 5.27 | 13.25 | 0.32 | 3.72 | 0.21 | 0.61 | 0.34 | 44.08 | 3.49 | 15.46 | | | X | X | X |
| HYD-12 | Zeolite | 19.65 | 9.41 | 0.90 | 0.16 | 0.52 | 0.02 | 0.60 | 0.02 | 50.93 | 0.14 | 16.39 | | | | X | |
| HYD-4 | Basalt | 14.66 | 10.46 | 13.15 | 0.12 | 6.13 | 0.23 | 2.34 | 0.24 | 48.95 | 2.27 | 2.19 | X | X | X | | X |
| *Other Samples* | | | | | | | | | | | | | | | | | |
| HYD-0 | Basalt | 14.53 | 10.63 | 13.84 | 0.31 | 6.21 | 0.20 | 2.40 | 0.19 | 49.71 | 2.68 | 1.40 | X | X | X | | X |
| HYD-1 | Laterite | 29.80 | 0.18 | 16.72 | 0.01 | 0.18 | 0.33 | 0.15 | 0.03 | 37.83 | 3.30 | 12.01 | | | X | | X |
| HYD-2 | Laterite | 21.47 | 0.14 | 36.64 | 0.01 | 0.14 | 0.04 | 0.05 | 0.32 | 23.39 | 5.49 | 12.02 | | | X | | X |
| HYD-3 | Saprolite | 10.21 | 7.90 | 15.01 | 0.43 | 5.05 | 0.15 | 0.48 | 0.27 | 38.18 | 2.96 | 11.78 | X | | X | X | X |

[a]Pyroxene.
[b]Plagioclase.
[c]Phyllosilicates.

the metal-OH bending vibrations in octahedral sites [*Bishop et al.*, 2002a, 2008b; *Farmer*, 1974; *Michalski et al.*, 2006]. A well-defined doublet from 550 to 400 $cm^{-1}$ due to Al and Fe substitution for Si and the Si(Al, Fe)$O_4$ bending vibrations is also characteristic of smectites [*Bishop et al.*, 2008b; *Michalski et al.*, 2006]. Compared with mid-IR spectra of basalt samples, the saprolite samples have a broader range of spectral features, consistent with these samples having differences in chemistry within the same broad smectite group. Differences in spectral features can help differentiate different clays, and mineral identifications are generally consistent with VNIR spectroscopy results. For example, Si(Al, Fe)$O_4$ bending vibrations shift from 540 to 535 $cm^{-1}$ (18.5–18.7 $\mu$m) in HYD-6 and HYD-8 to 528–519 $cm^{-1}$ (18.9–19.3 $\mu$m) in HYD-3, HYD-9 and HYD-10. The frequency of this vibration indicates that HYD-6 and HYD-8 contain more Al-rich smectites, while the other samples contain more Fe- and Mg-rich smectites [*Michalski et al.*, 2005; *Stubican and Roy*, 1961].

[26] The positions of the Christiansen features of the two zeolite samples are approximately 1260 $cm^{-1}$ (7.94 $\mu$m) in HYD-7 and 1245 $cm^{-1}$ (8.03 $\mu$m) in HYD-12 (Figure 6c) [*Cloutis et al.*, 2002]. Asymmetric Si-O stretches occur at 1190–1000 $cm^{-1}$ (8.4–10 $\mu$m) and are maximized at slightly shorter wavenumber (1043 $cm^{-1}$ or 9.59 $\mu$m) for HYD-12 than HYD-7 (1066 $cm^{-1}$ or 9.38 $\mu$m) [*Cloutis et al.*, 2002]. The wavelengths of both sets of features are consistent with HYD-12 having a higher Al:(Al + Si) ratio than HYD-7 [*Cloutis et al.*, 2002]. O-Si-O and O-Al-O bending vibrations occur at 625–400 $cm^{-1}$ (16–25 $\mu$m) [*Cloutis et al.*, 2002].

[27] Spectra of all laterite samples (HYD-13 is shown in Figure 6d) are also consistent with a mixture of kaolin minerals and Fe-oxides. Christiansen features are fairly uniform and range from 1183 $cm^{-1}$ to 1153 $cm^{-1}$ (8.45–8.67 $\mu$m). Pure Al-phyllosilicates generally have a Christiansen feature near ~1235 $cm^{-1}$ (8.1 $\mu$m) [*Bishop et al.*, 2008b]. The shift to shorter wavenumber results from the presence of Fe-oxides that are intimately mixed with kaolinite or halloysite. The shape and position of the Reststrahlen bands are consistent with kaolinite [e.g., *Bishop et al.*, 2008b; *Farmer*, 1974] and are not affected by Fe-oxides, which are featureless at 1500–650 $cm^{-1}$ (6.67–15.4 $\mu$m) [*Christensen et al.*, 2000a]. Absorption features at 625–400 $cm^{-1}$ (16–25 $\mu$m) result from the convolution of Al-O-Si vibrations of kaolinite [*Bishop et al.*, 2008b; *Farmer*, 1974] and metal-O stretching vibrations in hematite [*Christensen et al.*, 2000a].

### 5.3. X-Ray Diffraction

[28] XRD results are summarized in Table 1, which shows the presence and absence of minerals in the samples (XRD results of selected samples are shown in Figure 7). For HYD-0, HYD-4, HYD-5, and HYD-11, the XRD-detected mineral assemblages of plagioclase and pyroxene with minor phyllosilicates and Fe/Ti-oxides are consistent with that expected for basalt (with minor alteration) and the spectroscopic measurements. XRD results show that all of the samples from the saprolite (HYD-3, HYD-6, HYD-8, HYD-9, and HYD-10) are dominated by phyllosilicates but have additional complexities. HYD-3 and HYD-10 have zeolites: chabazite, stilbite, and levyne in HYD-3 and chabazite and stilbite in HYD-10. Additional analyses on HYD-9 show that the clay fraction is interlayered illite/smectite, ordered and 70% expandable. HYD-3 contains augite and HYD-8, in the middle of the section, has some pigeonite and andesine, but these minerals are not apparent in the spectra. XRD data show that HYD-7 is stilbite and HYD-12 is a mixture of chabazite, stilbite, and heulandite, consistent with zeolites identified spectroscopically. Of the laterite samples, HYD-1 is mostly kaolinite with some hematite and a small amount of ilmenite and magnesioferrite, HYD-2 is kaolinite and goethite with some anatase and rutile, and HYD-13 is kaolinite, goethite, and hematite.

### 5.4. Major Element Chemistry and Loss on Ignition

[29] Major element chemistry of all samples is shown in Table 1. The major element compositions of HYD-0, HYD-4, HYD-5, and HYD-11 are all consistent with Ambenali formation Deccan basalts [*Beane et al.*, 1986; *Kısakürek et al.*, 2004]. All of those samples have losses on ignition that are less than 2.2 wt %, which would be characteristic of mostly fresh basalt or basalt mixed with

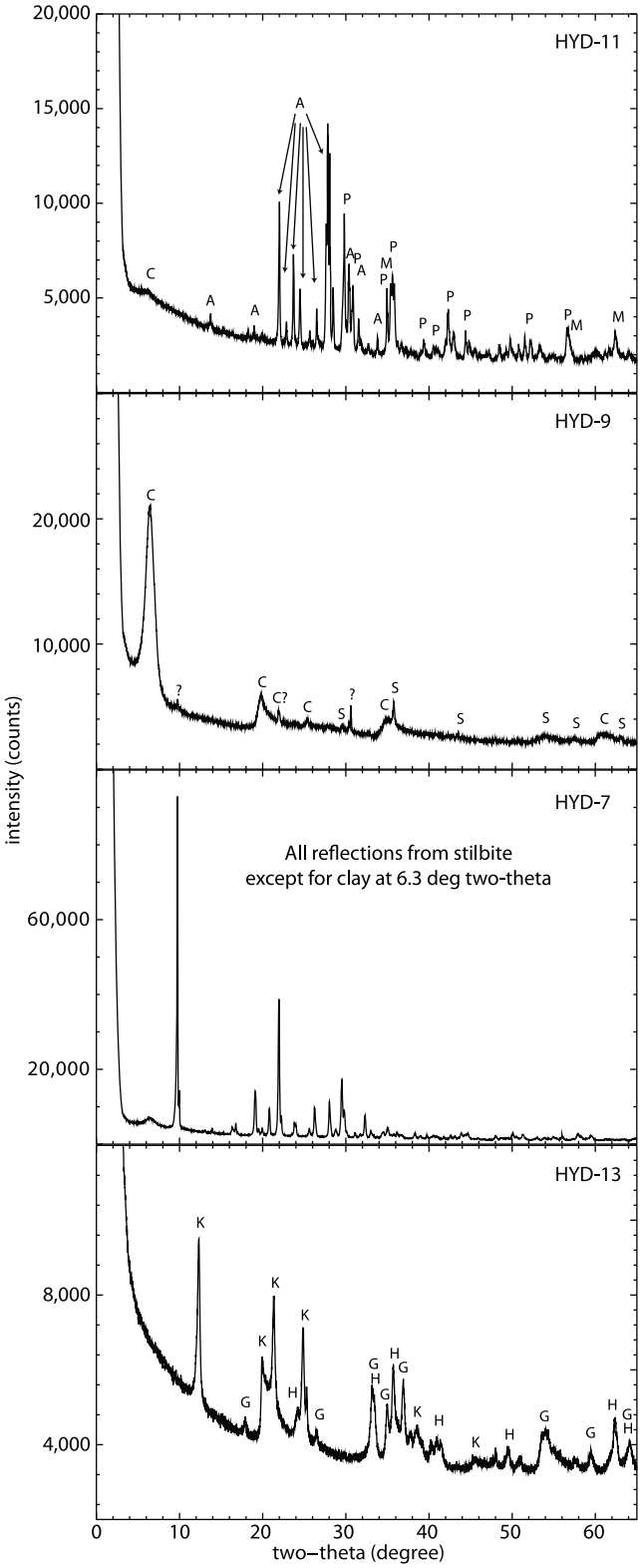


**Figure 7.** Example XRD spectra of 4 samples: (from top to bottom) HYD-11 (basalt), HYD-9 (saprolite), HYD-7 (zeolite), and HYD-13 (laterite). C = clay, A = plagioclase (anorthite), P = pyroxene, M = magnetite, K = kaolinite, G = goethite, S = spinel, H = hematite, and ? = unknown.

a small amount of altered hydrated minerals. Chemistries of HYD-3, HYD-6, HYD-8, HYD-9, and HYD-10 from the saprolite from ICP-AES show that Na, Ca, Mg, and Si are depleted and Ti is slightly enriched relative to the basalts, consistent with leaching (Table 1). Element-mass transfer coefficients [*Anderson et al.*, 2002] show that all elements have been depleted relative to the underlying basalt samples except K, which occurs in very low concentrations in all samples. The depletions suggest mass loss in the saprolite during alteration. HYD-8 has the highest Na, which is probably in the andesine in the sample. These saprolite samples have high volatile contents, with LOI values ranging from 11.78 wt % in HYD-3 to 19.17 wt % in HYD-9. Major element chemistries of HYD-7 and HYD-12 are consistent with reported zeolite chemistries [*Cloutis et al.*, 2002] and are dominated by Al, Ca, and Si with a small amount of Na and Mg (Table 1). The zeolites precipitated from the solution that altered the original basalt, so their chemistry reflects those elements that were leached from the basalt and are depleted in the saprolite. Relative Al:(Al + Si) and Ca:Na ratios interpreted from spectroscopy data are confirmed by the chemistry data. HYD-12 has higher Ca:Na and Al:(Al + Si) than HYD-7 as predicted. The small (<2 wt %) amount of Fe present in the ICP-AES results is likely contamination from the clay matrix surrounding the zeolites and is not part of the zeolite structure. The LOI of these samples is 16–18 wt %, probably mostly $H_2O$ in the zeolites' structures. The laterite samples (HYD-1, HYD-2, and HYD-13) are the most extensively leached. Ca, Na, K, and Mg are absent, and Si is low relative to basalt. Absolute concentrations of Fe, Al, and Ti are enriched relative to the underlying basalts, consistent with this unit containing only the most immobile elements, and element-mass transfer coefficients show enrichments, indicating possible transport of those elements upward in the section or from the surrounding landscape to this laterite. These samples have a LOI of 12–13 wt %, which is lower than most saprolite and zeolite samples but still represents a significant volatile content. These LOI values are comparable with those reported for pure kaolinite samples [e.g., *Bishop et al.*, 2008b; *Galan et al.*, 1998]. Some reported values for sedimentary hematite [e.g., *Chan et al.*, 2004] are very low (<5%).

### 5.5. Mössbauer Spectroscopy

[30] Mössbauer parameters of fits to the spectra are given in Table 2, and example fits are shown in Figure 8. There was too little Fe in HYD-7 and HYD-12 for Mössbauer analysis, but all other samples were measured with this technique. In the basalt samples (HYD-0, HYD-4, HYD-5, and HYD-11), Mössbauer spectroscopy identifies Fe-bearing phases including ilmenite, oxidized pyroxene (clinopyroxene and orthopyroxene), and possibly olivine. HYD-4 has significant Fe-oxides, probably lepidocrocite or hematite, and HYD-11 contains magnetite. Mössbauer spectroscopy is consistent with $Fe^{3+}$ in phyllosilicates in all of the saprolite samples (HYD-3, HYD-6, HYD-8, HYD-9, and HYD-10). HYD-10, HYD-8, and HYD-6 all have some ilmenite. Other than in ilmenite, which is very resistant to weathering, there is no $Fe^{2+}$ in any of the samples except for HYD-3, which has some $Fe^{2+}$ in pyroxene. This is roughly consistent with XRD results, though Mössbauer does not detect pyroxene in HYD-8 (probably due to heavy peak

**Table 2.** Mössbauer Parameters of Deccan Trap Samples[a]

| | Sample | HYD-0 Basalt | HYD-4 Basalt | HYD-5 Basalt | HYD-11 Basalt | HYD-3 Saprolite | HYD-6 Saprolite | HYD8 Saprolite | HYD-9 Saprolite | HYD-10 Saprolite | HYD-1 Laterite | HYD-2 295K Laterite | HYD-2 4K Laterite | HYD-13 Laterite |
|---|---|---|---|---|---|---|---|---|---|---|---|---|---|---|
| $Fe^{3+}$ in pyroxene or clay | IS | 0.48 | 0.39 | 0.32 | 0.40 | 0.36 | 0.36 | 0.36 | 0.36 | 0.35 | 0.32 | 0.45 | | 0.37 |
| | QS | 0.70 | 0.53 | 0.60 | 0.61 | 0.67 | 0.56 | 0.55 | 0.61 | 0.55 | 0.49 | 0.91 | | 0.57 |
| | Width | 0.77 | 0.73 | 0.59 | 0.80 | 0.62 | 0.58 | 0.55 | 0.60 | 0.57 | 0.95 | 1.04 | | 0.46 |
| | Area | 0.18 | 0.17 | 0.23 | 0.15 | 0.49 | 0.68 | 0.60 | 0.60 | 0.67 | 0.21 | 0.39 | | 0.40 |
| $Fe^{2+}$ in ilmenite | IS | 1.04 | 1.07[b] | 1.09 | 1.06[b] | | 1.06 | 1.06[b] | | 1.06[b] | 1.07 | | | |
| | QS | 0.69 | 0.68[b] | 0.53 | 0.63 | | 0.62 | 0.68 | | 0.65 | 0.70 | | | |
| | Width | 0.38 | 0.30[b] | 0.43 | 0.46 | | 0.48 | 0.50 | | 0.45 | 0.36 | | | |
| | Area | 0.09 | 0.02 | 0.11 | 0.03 | | 0.05 | 0.06 | | 0.09 | 0.14 | | | |
| $Fe^{2+}$ in olivine/pyroxene | IS | 1.15 | 1.17 | 1.14 | 1.14 | | | | | | | 0.64 | | |
| | QS | 2.69 | 2.50 | 2.59 | 2.56 | | | | | | | 5.31 | | |
| | Width | 0.30[b] | 0.30[b] | 0.30[b] | 0.30[b] | | | | | | | 1.33 | | |
| | Area | 0.25 | 0.07 | 0.16 | 0.05 | | | | | | | 0.27 | | |
| $Fe^{2+}$ in pyroxene | IS | 1.10 | | 1.09 | | | | | | | | | | |
| | QS | 1.72 | | 1.71 | | | | | | | | | | |
| | Width | 0.36 | | 0.30[b] | | | | | | | | | | |
| | Area | 0.19 | | 0.12 | | | | | | | | | | |
| $Fe^{2+}$ in pyroxene | IS | 1.13 | 1.15 | 1.14 | 1.14 | 1.17 | | | | | | | | |
| | QS | 2.00 | 2.00 | 2.00 | 2.02 | 2.02 | | | | | | | | |
| | Width | 0.24[b] | 0.47 | 0.24[b] | 0.46 | 0.44 | | | | | | | | |
| | Area | 0.29 | 0.47 | 0.39 | 0.47 | 0.07 | | | | | | | | |
| Fe oxide | IS | | 0.44 | | 0.65 | 0.37 | 0.41 | | | | 0.37 | −0.21 | 0.48 | 0.35 |
| | QS | | −0.13 | | 0.32 | −0.22 | −0.12 | | | | −0.16 | 0.89 | −0.21 | −0.18 |
| | $B_{Hf}$ | | 409.1 | | 456.9 | 508.7 | 436.2 | | | | 469.3 | 300.8 | 479.4 | 463.8 |
| | Width | | 0.99 | | 0.52 | 0.30[b] | 0.97 | | | | 0.61 | 1.89 | 0.73 | 0.60[b] |
| | Area | | 0.15 | | 0.21 | 0.25 | 0.13 | | | | 0.20 | 0.34 | 0.19 | 0.12 |
| Fe oxide | IS | | 0.32 | | 0.28 | 0.36 | 0.30 | 0.33 | 0.32 | 0.31 | 0.37 | | 0.48 | 0.38 |
| | QS | | −0.01 | | 0.00 | −0.22 | −0.01 | −0.01 | 0.02 | −0.01 | −0.18 | | −0.25 | −0.21 |
| | $B_{Hf}$ | | 449.8 | | 488.6 | 496.2 | 499.6 | 497.1 | 495.1 | 496.3 | 505.4 | | 507.4 | 510.1 |
| | Width | | 0.45 | | 0.28 | 0.50 | 0.44 | 0.50 | 0.57 | 0.50 | 0.34 | | 0.99 | 0.28 |
| | Area | | 0.12 | | 0.09 | 0.19 | 0.15 | 0.35 | 0.18 | 0.24 | 0.45 | | 0.81 | 0.48 |
| | $\chi^2$ | 745.5 | 3807.0 | 904.4 | 3293.7 | 1398.9 | 2105.9 | 2023.6 | 1912.5 | 1878.3 | 2498.0 | 10842.1 | 11632.0 | 5084.2 |
| | $\lvert\chi^2\rvert$ | 1.46 | 7.44 | 1.77 | 6.44 | 2.72 | 4.12 | 3.95 | 3.73 | 3.67 | 4.88 | 21.18 | 22.73 | 9.88 |

[a]IS = isomer shift, in mm/s. QS = quadrupole splitting, in mm/s. Width given as FWHM, in mm/s. Area given as a fraction of total area = 1.
[b]Parameter fixed.

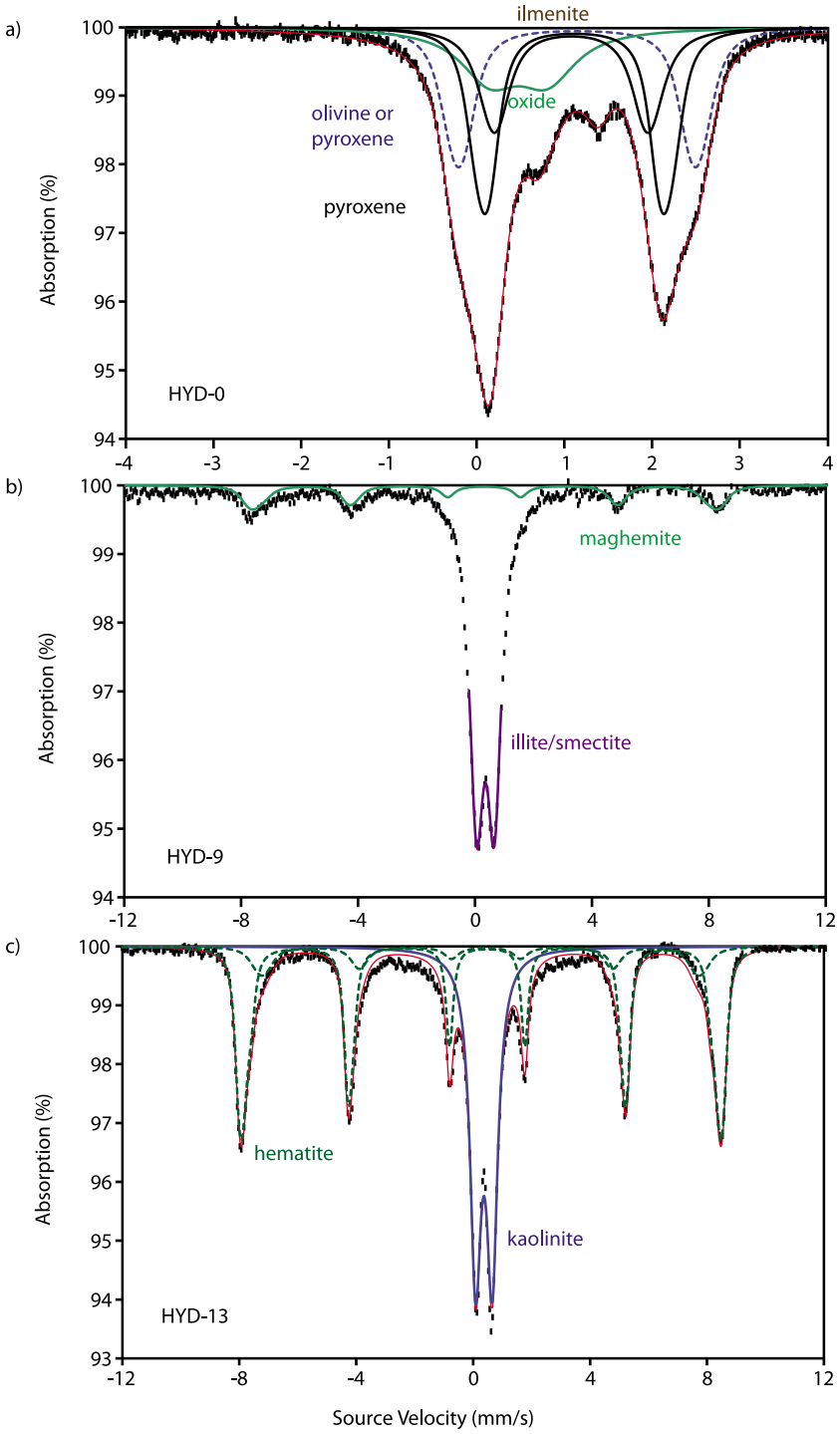


**Figure 8.** (a) Mössbauer spectrum of sample HYD-0. (b) Mössbauer spectrum of sample HYD-9. (c) Mössbauer spectrum of sample HYD-13. Although Mössbauer spectra do not unequivocally identify silicate minerals, peaks corresponding to olivine and/or pyroxene, ilmenite, kaolinite, and illite/smectite can be identified based on XRD results from the same rocks. Iron oxides such as hematite and maghemite can be fingerprinted using this technique.

overlap). HYD-3 contains hematite, but the other saprolite samples all contain maghemite. Mössbauer spectra of the laterite samples (HYD-1, HYD-2, and HYD-13) look similar to the saprolite samples. The spectra are consistent with the presence of $Fe^{3+}$ in an octahedral site in a clay mineral, which may suggest some Fe substitution in the kaolinite [*Iriarte et al.*, 2005; *Petit et al.*, 1999]. In contrast to the saprolite samples which generally contain maghemite, Mössbauer spectra of the laterite samples show hematite. There is no $Fe^{2+}$ in these samples, indicating that all Fe, including in ilmenite, has been oxidized.

### 5.6. Summary

[31] The least-altered samples are HYD-0, HYD-4, HYD-5, and HYD-11. All analyses of these samples are consistent with weakly altered basalts. These basalts contain higher-Ca pyroxenes such as pigeonite or augite based on both spectroscopy and XRD. Mössbauer results indicate that the pyroxene has been somewhat oxidized and HYD-4 has significant Fe-oxides. The oxidation of these samples could be the product of weathering and exposure to oxidizing conditions at the surface. Plagioclase, identified by XRD, cannot be seen in VNIR spectra of these samples, which is expected since plagioclase can only be detected with VNIR spectroscopy at concentrations greater than 85% [*Crown and Pieters*, 1987]. The presence of plagioclase can be inferred from the mid-IR spectra, and major element chemistry analysis indicates the presence of Al, likely concentrated in the plagioclase. Concentrations of more mobile elements such Na, Ca, and Mg in these samples, consistent with other reported Deccan basalt chemistries [e.g., *Beane et al.*, 1986], indicate that these samples have undergone little leaching. Relative degrees of the alteration products that are present within these samples can be seen in the spectroscopy and are consistent with other laboratory analyses. The band depths and positions of vibrational absorption features and LOI of HYD-4 and HYD-5 suggest that they have been the most altered, and their spectra indicate that they may have small amounts of chlorite, Fe-smectite, or other phyllosilicate minerals in them.

[32] The smectite-bearing section of this profile, which is intermediate in terms of the degree of leaching, is the saprolite. Mineral identifications from VNIR and mid-IR spectra are generally consistent for each sample. HYD-3 and HYD-10 have Fe-rich smectite clays. Both samples also have zeolites, which can be seen in ASD spectra of the largest particle size separates and the unground samples. The presence of zeolites probably affects the Christiansen feature position in the mid-IR, especially for HYD-10. The Christiansen feature of HYD-3 is at the longest wavelength, which may suggest that this sample is less altered than the other saprolite samples, consistent with the detection of pyroxene in the sample by XRD and Mössbauer spectroscopy. HYD-9 appears to be the most altered, has the deepest 1.9 $\mu$m absorption feature and largest LOI, and is a mixture of Al, Fe, and Mg smectites. HYD-8 occurs stratigraphically and is mottled with HYD-9 but appears to be less altered than HYD-9. HYD-8 and HYD-6 contain a mixture of Al-bearing smectites such as montmorillonite and Fe-bearing smectites such as nontronite. HYD-8 also contains some pyroxene and plagioclase, which VNIR spectroscopy does not detect. XRD results of all samples are consistent with these samples containing phyllosilicates but suggest that the types of phyllosilicates may be more complex, such as illite/smectite rather than pure smectite as VNIR and mid-IR spectroscopy suggest. Major element chemistry shows that these samples have been incompletely leached and still have some mobile cations remaining, but they are leached somewhat relative to the basalts. Changes in the spectroscopy from basalt to saprolite reflect changes in the mineralogy and chemistry of the samples.

[33] There are also zeolites throughout the saprolite that formed through precipitation from solution and possible low-grade hydrothermal alteration. As a result, their major element chemistries are dominated by the most mobile elements in the original basalts because these are the cations that were leached and mobilized soon after emplacement. VNIR and mid-IR spectroscopy shows that HYD-7 and HYD-12 are zeolites, based on the presence of fundamental and combination and overtone features from $H_2O$ and OH. The positions of absorption features in spectra of these samples can be used successfully to determine relative Na, Ca, Al, and Si contents in the samples, and these results are confirmed by ICP-AES analyses. The combination of zeolite minerals present in HYD-12 cannot be distinguished with spectroscopy and can only be identified by XRD. Zeolite samples can best be distinguished from saprolite samples in VNIR spectroscopy by the lack of metal-OH combination bands in the zeolite spectra and the additional absorptions from $H_2O$ at 0.970–0.975 and 1.161–1.163 $\mu$m in the zeolites. Zeolites in HYD-3 and HYD-10 (saprolite samples) are surrounded by clays and can only be seen spectroscopically in the largest particle size separates and the whole rock. Since the absorption features in the zeolites overlap with those from smectites in the VNIR, it is difficult to identify the zeolites that are mixed with smectite in these samples, although the zeolites probably do deepen absorption features due to $H_2O$. Mid-IR spectra of the pure zeolite samples have Christiansen features at a longer wavenumber (1260–1230 $cm^{-1}$) than the saprolites (1230–1180 $cm^{-1}$). The zeolites in the saprolite samples probably also affect the major element chemistry and LOI results, but it is difficult to distinguish the effects of zeolites from heterogeneities in the phyllosilicates. XRD readily identifies zeolites in HYD-3 and HYD-10 as well as the pure zeolite samples.

[34] All analyses of the laterite samples are consistent with a kaolinite and hematite or goethite assemblage. VNIR spectroscopy perhaps shows the assemblage best because distinct Fe-oxide and kaolinite absorption features can be seen. Mid-IR spectra also show the assemblage, particularly using methods such as deconvolution, but the kaolinite and hematite absorption features overlap, making the hematite difficult to distinguish visually. Major element chemistry data show that only the most immobile elements (Fe, Al, Ti, some Si) are present in these samples and more mobile elements (Na, Ca, K, Mg) are absent. The Mössbauer data do not identify kaolinite but confirm Fe-oxide identifications from other analyses.

## 6. Discussion

[35] We examined the composition of weathering horizons that formed through leaching in a basaltic environment and focused in particular on how the weathering processes translate to remotely sensed signatures. Three main types of units were present, basalt, saprolite, and laterite, and each has a unique spectral signature at VNIR and mid-IR wavelength ranges (Figure 9). In the visible and near infrared, the crystal field absorptions from $Fe^{2+}$ in pyroxene in the basalts disappear when the basalts are altered and leached and absorption features at 1.4 and 1.9 $\mu$m from OH and $H_2O$ appear along with metal-OH combination bands near 2.2–2.3 $\mu$m and the continuum is modified. The OH stretching vibrations at 2.7–2.8 $\mu$m also deepen and sharpen. In the mid-IR, overlapping Si-O vibrations due to plagioclase and

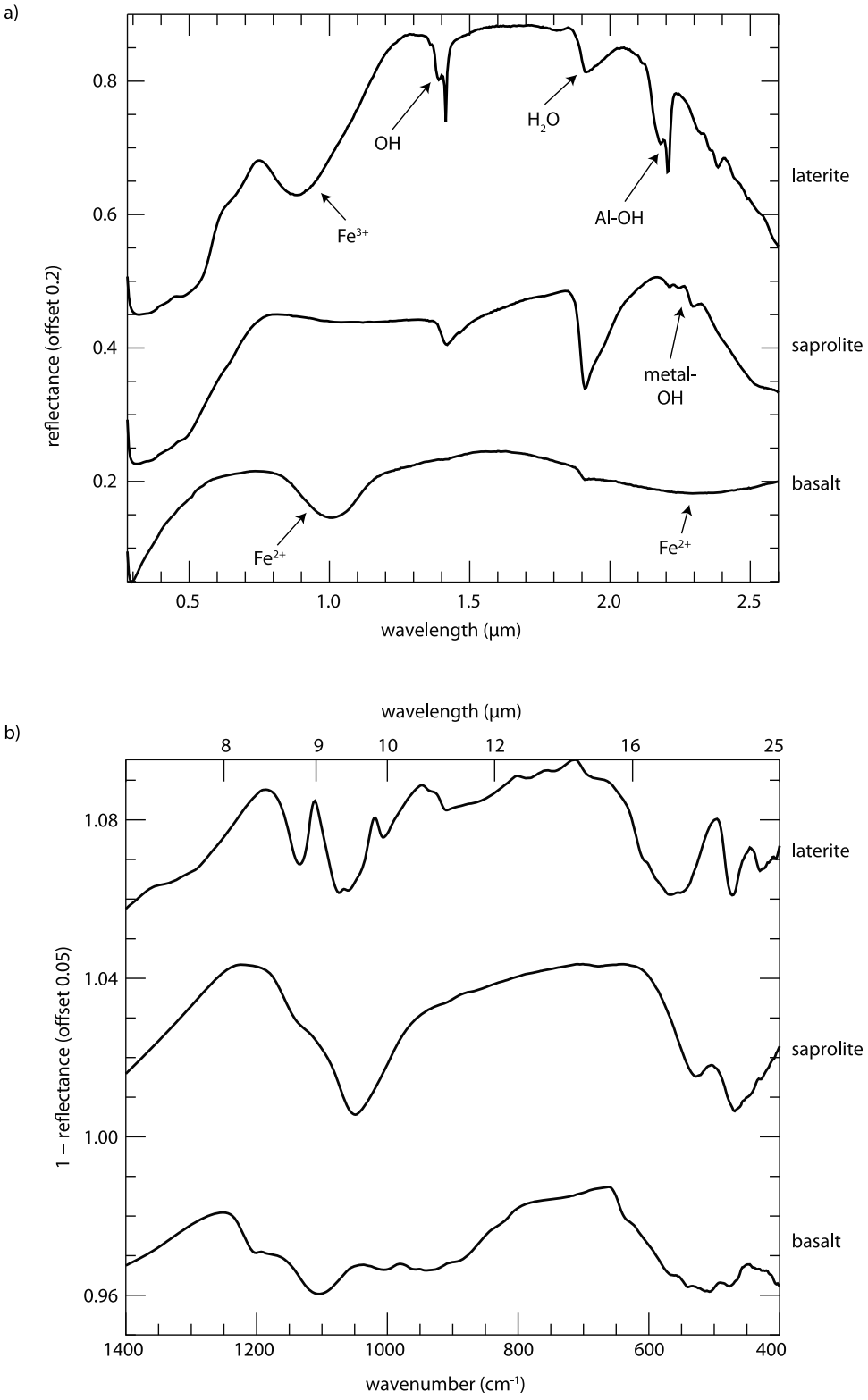


**Figure 9.** Example spectra of three main units in the (a) VNIR and (b) mid-IR: basalt (HYD-11), saprolite (HYD-9), and laterite (HYD-13).

pyroxene in the basalt are replaced by a single sharper absorption indicative of phyllosilicates. As the saprolite weathers to a laterite, the 1.4 $\mu$m absorption feature becomes a doublet, and there is a second doublet at 2.2 $\mu$m from Al-OH diagnostic of kaolinite. Since there is no molecular $H_2O$ in the kaolinite structure, the 1.9 $\mu$m band depth decreases but, in these samples, does not disappear, probably due to the presence of adsorbed water, halloysite, or a small amount

of another phyllosilicate such as smectite that does have molecular $H_2O$. Crystal field absorptions reappear but are at shorter wavelengths than those in the basalt samples and are due to $Fe^{3+}$ in ferric oxides. The OH vibration at 2.7–2.8 $\mu$m becomes a well-defined triplet. In the mid-IR, the single main absorption in the saprolite becomes several absorption features at wavelengths consistent with kaolinite. These visible, near IR, and mid-IR spectroscopic changes are directly related to the degree of leaching of the samples, as basalt is altered and slightly leached to smectite, which is leached to kaolinite. While the direct smectite to kaolinite transformation could not be sampled in this particular vertical section due to a lack of exposed outcrop, Figure 10a shows that, based on the major element chemistry of the samples, the smectite-dominated saprolite represents an intermediate step between the mostly unaltered basalt and the fully leached kaolinite. Furthermore, other studies of weathering profiles formed on basalt have smectite-bearing zones between the unaltered basalt and the kaolinite- or gibbsite-bearing laterite [e.g., *Hill et al.*, 2000; *Nesbitt and Wilson*, 1992; *Taylor et al.*, 1992]. The pathways from leaching of basalt to smectite (saprolite) to kaolinite (laterite) are well-represented in this vertical section, and the chemistry data and changes in mobile element concentrations confirm this leaching relationship (Figure 10). Figure 10b shows element-mass transfer coefficients ($\tau$) of four elements in the profile. These coefficients are enrichments and depletions of four measured elements relative to the underlying basalt and the most immobile element measured, Ti [*Nesbitt and Wilson*, 1992], following the methods of *Anderson et al.* [2002], *Brimhall and Dietrich* [1987], and *Jin et al.* [2010]. CaO ($Na_2O$ and MgO show similar trends), $SiO_2$, $Al_2O_3$, and $Fe_2O_3$ are all depleted, providing evidence for possible mass loss in the saprolite during the weathering process. The most mobile elements (Ca, Na, and Mg) have been removed in the laterite, and $SiO_2$ is depleted in the laterite, while $Fe_2O_3$ and $Al_2O_3$ have been enriched, possibly through transport upward in the profile or lateral transport through the surrounding landscape to the laterite before the surface around the laterite cap was eroded and lowered. These chemical trends of enrichments and depletions could be present on Mars if the kaolinite over Fe/Mg-smectite stratigraphy indeed formed through leaching.

[36] The laterite in this vertical section is the most leached horizon. Spectroscopic measurements clearly show the kaolinite and hematite or goethite assemblage confirmed by other chemical and mineralogical analyses. The agreement between the spectroscopy results and other laboratory analyses provides good confidence for interpretation of similar units on Mars with CRISM and OMEGA.

[37] All analyses of the laterite samples show a clear association between hematite or goethite and kaolinite. The abundance of Fe-oxides is striking and is as integral to the signatures of intense leaching in the laterite as the kaolinite. We do not see kaolinite without Fe-oxides in any of our samples. Laterites formed from a basaltic protolith elsewhere on Earth have the same characteristic kaolinite and Fe-oxide (usually hematite or goethite) assemblage [e.g., *Nesbitt and Wilson*, 1992]. In some weathering profiles, additional leaching has removed much Si, forming a gibbsite and Fe-oxide assemblage with some remaining kaolinite [*Hill et al.*, 2000; *Taylor et al.*, 1992]. Based on the association with Fe-oxides, this and other laterites formed in an oxidizing environment in a zone with frequent interaction with the atmosphere. Reducing conditions would have mobilized and removed the Fe. Kaolinite formation requires leaching by relatively fresh water with low silica and base cation activities, so input of meteoric waters, as opposed to solely groundwater, promotes the formation of kaolinite over smectite [e.g., *Wilson*, 1999]. On Mars, the presence of kaolinite, if formed through leaching, would similarly require freshwater. Possible sources include rainfall or melting of snow or ice. For kaolinite to form through leaching on Mars, surface temperatures would need to have been above freezing over an extended period to allow for freshwater to be stable and leach the primary and secondary minerals, but the exact temperature requirements are unconstrained. Alternatively, there may have been only transient heating leading to basal melting of ice deposits or melting of snow. On Earth, laterites can form in warm, wet, often tropical climates [*Hill et al.*, 2000; *Kısakürek et al.*, 2004], but they have also formed in cooler climates at slower rates [*Taylor et al.*, 1992]. Several hypotheses have been suggested for formation of laterites. Laterites may be a residual layer of Al-, Fe-, and Ti-bearing minerals after all of the more mobile elements have been removed through in situ leaching [*Widdowson and Cox*, 1996]. These laterites are resistant to erosion and now form caps as material around them has been removed [*Jay and Widdowson*, 2008; *Widdowson and Cox*, 1996]. Others have suggested that Fe is leached in the subsurface from a region, is transported laterally, and precipitates when it reaches oxidizing conditions in paleoriver channels to form laterites or ferricretes, which are now in inverted relief [*Ollier and Sheth*, 2008; *Pain and Oilier*, 1995]. Both of these hypotheses involve leaching, either horizontally or vertically, and are mechanisms that could have operated on Mars. However, the laterally extensive nature of the kaolinite deposits on Mars suggests that they formed through in situ leaching. It has also been suggested that the enrichment of Fe in laterites on Earth is only possible due to biological activity, which could explain differences between Earth and Mars. Plants and microbes can reduce Fe, increase the acidity of leaching solutions, and complex and chelate Fe, all of which make Fe more mobile [*Duchaufour and Souchier*, 1978; *Pate et al.*, 2001]. Ferricretes could even be bio-precipitates [*Duchaufour and Souchier*, 1978]. A complementary type of weathering profile formed from serpentinized peridotite and studied as an analog for Mars has a similar laterite horizon with kaolinite and Fe-oxides [*Gaudin et al.*, 2011]. Taken with our results, mafic and ultramafic rocks leached to kaolinite in an oxidizing environment should have an intimate association with Fe-oxides. On Mars, we would therefore expect to see Fe-oxides associated with kaolinite that overlies Fe/Mg-smectite if these deposits formed through leaching under oxidizing conditions. The same association with Fe-oxides should be present if the environment was oxidizing where montmorillonite overlies Fe/Mg-smectite on Mars if the montmorillonite is the product of leaching. CRISM data of kaolinite and montmorillonite deposits on Mars show locations where Al-phyllosilicates co-occur with Fe-oxides in Mawrth Vallis, although the Fe-oxide contents of the deposits vary [*McKeown et al.*, 2009; *Wray et al.*, 2008]. A detailed assessment of Mars data is beyond the scope of this paper but is the subject of a future paper.

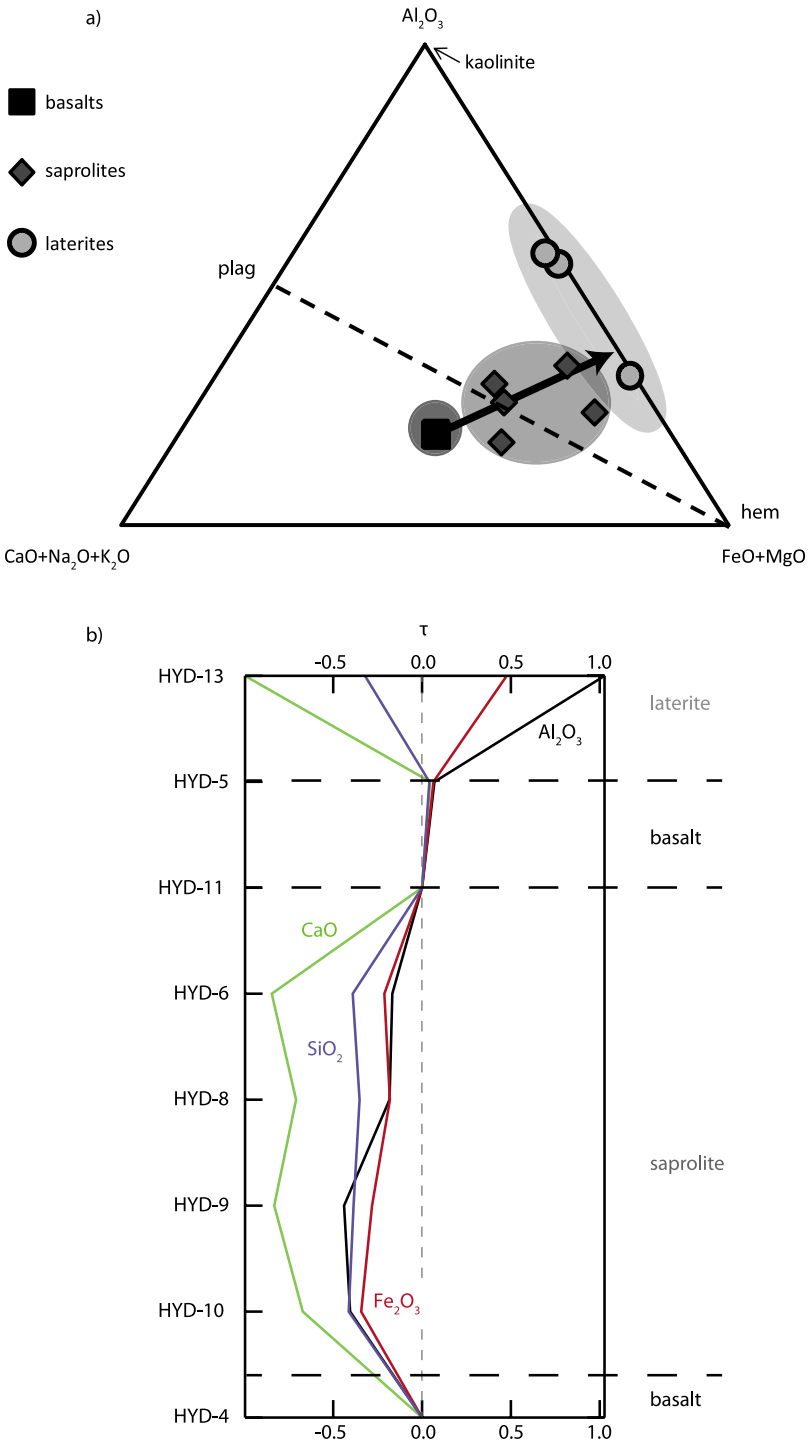


**Figure 10.** (a) Ternary diagram showing the progressive leaching of these altered Deccan basalts. The arrow shows the progression from basalt to saprolite to laterite in major element chemistry. Data are in mole % oxide. Plagioclase (plag), kaolinite, and hematite (hem) are shown for reference, and unaltered basalts should plot below the dashed line [after *Nesbitt and Wilson*, 1992]. (b) Mass transfer coefficients ($\tau$) of CaO, $SiO_2$, $Al_2O_3$, and $Fe_2O_3$ in samples in stratigraphic order calculated following the methods of *Anderson et al.* [2002] and *Jin et al.* [2010] relative to Ti (assumed to be immobile) and the underlying basalts. Values for HYD-6-10 are relative to HYD-4, and HYD-5 and HYD-13 are relative to HYD-11. Values less than 0 are depletions, and values greater than 0 are enrichments. $Na_2O$ and MgO (not shown) show a similar trend to CaO.

[38] Understanding the composition of the saprolite is less clear. Spectra of smectites on Mars generally have one metal-OH combination tone and are often interpreted as a single smectite, either Fe/Mg-bearing or Al-bearing [e.g., *Bishop et al.*, 2008a; *Ehlmann et al.*, 2009]. It has also been suggested that these clays are mixed layer clays or vermiculite [*Carter and Poulet*, 2012; *Milliken and Bish*, 2010; *Milliken et al.*, 2010]. Spectra of the Deccan saprolite samples are complicated, with multiple overlapping absorptions from different types of metal-OH coordination. Since these samples formed from weathering of pyroxene, plagioclase, and other minerals in basalt, it is most likely that these samples are intimate mixtures of multiple types of clays. There may also be mixed-layer clays, as XRD suggests for one sample. Spectra of these clays are further complicated by the presence of zeolites in some samples, which may enhance the strength of the 1.4 and 1.9 $\mu$m OH and $H_2O$ overtones and combination tones but, at the smallest particles sizes, are not detectable spectroscopically unless the samples are pure zeolites. Nevertheless, the presence of zeolites is important in understanding the aqueous history of these samples because zeolites form through both low-grade metamorphism and low-temperature, alkaline alteration processes [*Ming and Mumpton*, 1989, and references therein]. Additionally, the presence of zeolites may inhibit the formation of kaolinite from smectite by contributing base cations to the waters in the soil and keeping activities high enough that kaolinite cannot precipitate [*Bhattacharyya et al.*, 1993, 1999, 2006]. The zeolites may help explain why such a thick smectite section remains here without the upper portion altering to kaolinite (or a laterite). Alternatively, the timeframe between the upper and lower lava flows, estimated to be less than one million years based on the magnetostratigraphy of the Deccan Traps [*Jay and Widdowson*, 2008], may have been too short for the extensive leaching required for kaolinite formation. Spectroscopic analyses do not show the presence of residual pyroxene in a couple saprolite samples, so laboratory spectroscopic measurements do not reveal the full mineral assemblages of these smectite-bearing samples. Spectroscopic observations of Mars have atmospheric contributions, instrument noise, and larger pixel sizes [e.g., *Murchie et al.*, 2007], which can make them more difficult to interpret. Clays on Mars may be similarly complex, with deposits not being pure Al-rich or Fe/Mg-rich smectite and likely containing a mixture of different phyllosilicates along with other minerals. It has also been suggested that mixed-layer clays may be better interpretations of CRISM data [*Milliken and Bish*, 2010; *Milliken et al.*, 2010]. *Poulet et al.* [2008] use nonlinear modeling of OMEGA spectra to calculate that Fe/Mg-smectite deposits in Mawrth Vallis contain 5–15% pyroxene and 25–35% plagioclase and in Nili Fossae have 20% pyroxene and 40–50% plagioclase. There may be other components in the clays, such as zeolites, that are difficult to identify in mixtures with smectites because the zeolite absorption features are due to $H_2O$ and overlap with smectite features. These other components (complex clays, pyroxene, zeolites, etc.) may not be present in the deposits observed by CRISM on Mars, but, based on the results here of measurements under laboratory conditions, should not be ruled out. The detection limit of thermal infrared spectroscopy of Mars is estimated to be 10–15% [*Christensen et al.*, 2000b]. Detection limits of VNIR spectroscopy are more difficult to determine and are highly dependent on the specific mineral of interest and its spectral contrast. Spectra of weathered soils on Earth and Mars are intimate mixtures of minerals and are affected by multiple scattering, where a single photon of light interacts with multiple minerals [e.g., *Hapke*, 1981]. As a result, it is difficult to derive abundances of the minerals present, and minor components may not be identified. The textures may also affect the spectral signatures more than the XRD pattern because the surface of grains within the sample, which dominate the spectra, may be altering to clays, while the interior may still be pristine primary minerals. These factors may help explain the differences between the XRD and spectroscopy results.

[39] Samples from the basalt layers show the classic crystalline igneous electronic absorption features seen across planetary bodies, including Mars, the moon, and asteroids [e.g., *Adams*, 1968; *Gaffey et al.*, 1993; *McCord et al.*, 1970]. Basaltic terrains have been identified across Mars, and the surface of Mars has undergone aqueous alteration. The starting material of our vertical section is a good analog for a major component of the Martian crust [*Christensen et al.*, 2000b]. The basalt layers are in close association with other intensely weathered zones (saprolite and laterite), yet the basalts show only minimal alteration signatures. Therefore, the presence of unaltered basalt on Mars does not necessarily preclude interaction with water. These layers had been buried when the weathering profiles and soils above them formed and were subsequently exposed via erosion or other processes (e.g., excavation in a quarry, which may be analogous to cratering processes exposing buried material). One interesting outstanding question is how these pristine layers of basalt remain despite conditions of extensive leaching and alteration. It is possible that these layers were not altered because waters became saturated as they moved further down in the soil and could no longer alter the deepest material. There may also have been changes in porosity and permeability downward in the soil that prevented water from reaching deeper into the soil and weathering the basalt.

## 7. Conclusions

[40] A vertical section of altered Deccan basalts was studied as an analog for the Al-phyllosilicate over Fe/Mg-smectite stratigraphy on Mars. In this section, a laterite is the most leached horizon and has a characteristic kaolinite and Fe-oxide assemblage. Interpretations of the spectroscopic data agree well with all other analyses. The presence of Fe-oxides with kaolinite would be expected on Mars if mafic or ultramafic rocks were leached under oxidizing conditions. The formation of kaolinite through leaching has implications for the climate of early Mars because kaolinite formation requires abundant liquid water. A thick saprolite has been incompletely leached, and spectroscopic signatures are dominated by complex smectite clays, with overlapping metal-OH combination bands. These clays are more complicated than those observed on Mars with a single metal-OH combination band, but smectites on Mars may be more complex than the presence or absence of single clay minerals often reported. Other laboratory analyses of the saprolite samples showed additional minerals that could not be identified with spectroscopy. Basalt samples showed the classic electronic transitions from $Fe^{2+}$ and were weakly altered, but crystalline

igneous rocks remained despite the abundance of water present since the basalts were emplaced.

[41] **Acknowledgments.** We are very grateful for the fine work of the NASA MRO project team and the fine job by the CRISM Science Operations Center (SOC). This work was supported by NASA through a subcontract through the Applied Physics Lab at Johns Hopkins University. We would like to thank Taki Hiroi for assistance with RELAB spectroscopic measurements, Dave Murray and Joe Orchardo for their help with flux fusion and ICP-AES, William Benzel at the USGS for his assistance with XRD analyses, and Mark Salvatore for helpful discussions and comments on a draft of this manuscript. Finally, we would like to thank two reviewers for their helpful reviews.

## References

Adams, J. B. (1968), Lunar and Martian surfaces: Petrologic significance of absorption bands in the near-infrared, *Science*, *159*(3822), 1453–1455, doi:10.1126/science.159.3822.1453.

Adams, J. B. (1974), Visible and near-infrared diffuse reflectance spectra of pyroxenes as applied to remote sensing of solid objects in the solar system, *J. Geophys. Res.*, *79*(32), 4829–4836, doi:10.1029/JB079i032p04829.

Altheide, T. S., V. F. Chevrier, and E. Noe Dobrea (2010), Mineralogical characterization of acid weathered phyllosilicates with implications for secondary Martian deposits, *Geochim. Cosmochim. Acta*, *74*(21), 6232–6248, doi:10.1016/j.gca.2010.08.005.

Anderson, S. P., W. E. Dietrich, and G. H. Brimhall (2002), Weathering profiles, mass-balance analysis, and rates of solute loss: Linkages between weathering and erosion in a small, steep catchment, *Geol. Soc. Am. Bull.*, *114*(9), 1143–1158, doi:10.1130/0016-7606(2002)114<1143:WPMBAA>2.0.CO;2.

Andrieux, P., and S. Petit (2010), Hydrothermal synthesis of dioctahedral smectites: The Al–Fe3+ chemical series, *Appl. Clay Sci.*, *48*(1–2), 5–17, doi:10.1016/j.clay.2009.11.019.

Beane, J. E., C. A. Turner, P. R. Hooper, K. V. Subbarao, and J. N. Walsh (1986), Stratigraphy, composition and form of the Deccan Basalts, Western Ghats, India, *Bull. Volcanol.*, *48*(1), 61–83, doi:10.1007/BF01073513.

Bhattacharyya, T., D. K. Pal, and S. B. Deshpande (1993), Genesis and transformation of minerals in the formation of red (Alfisols) and black (Inceptisols and Vertisols) soils on Deccan basalt in the Western Ghats, India, *J. Soil Sci.*, *44*(1), 159–171, doi:10.1111/j.1365-2389.1993.tb00442.x.

Bhattacharyya, T., D. Pal, and P. Srivastava (1999), Role of zeolites in persistence of high altitude ferruginous Alfisols of the humid tropical Western Ghats, India, *Geoderma*, *90*(3–4), 263–276, doi:10.1016/S0016-7061(98)00122-0.

Bhattacharyya, T., D. K. Pal, S. Lal, P. Chandran, and S. K. Ray (2006), Formation and persistence of Mollisols on zeolitic Deccan basalt of humid tropical India, *Geoderma*, *136*(3–4), 609–620, doi:10.1016/j.geoderma.2006.04.021.

Bibring, J.-P., et al. (2005), Mars surface diversity as revealed by the OMEGA/Mars Express observations, *Science*, *307*(5715), 1576–1581, doi:10.1126/science.1108806.

Bibring, J.-P., et al. (2006), Global mineralogical and aqueous Mars history derived from OMEGA/Mars Express data, *Science*, *312*(5772), 400–404, doi:10.1126/science.1122659.

Bishop, J. L., C. M. Pieters, and J. O. Edwards (1994), Infrared spectroscopic analyses on the nature of water in montmorillonite, *Clays Clay Miner.*, *42*(6), 702–716, doi:10.1346/CCMN.1994.0420606.

Bishop, J., J. Madejová, P. Komadel, and H. Fröschl (2002a), The influence of structural Fe, Al and Mg on the infrared OH bands in spectra of dioctahedral smectites, *Clay Miner.*, *37*(4), 607–616, doi:10.1180/0009855023740063.

Bishop, J. L., P. Schiffman, and R. Southard (2002b), Geochemical and mineralogical analyses of palagonitic tuffs and altered rinds of pillow basalts in Iceland and applications to Mars, *Geol. Soc. Spec. Publ.*, *202*(1), 371–392, doi:10.1144/GSL.SP.2002.202.01.19.

Bishop, J. L., P. Schiffman, E. Murad, M. D. Dyar, A. Drief, and M. D. Lane (2007), Characterization of alteration products in tephra from Haleakala, Maui: A visible-infrared spectroscopy, Mössbauer spectroscopy, XRD, EMPA and TEM study, *Clays Clay Miner.*, *55*(1), 1–17, doi:10.1346/CCMN.2007.0550101.

Bishop, J. L., et al. (2008a), Phyllosilicate diversity and past aqueous activity revealed at Mawrth Vallis, Mars, *Science*, *321*(5890), 830–833, doi:10.1126/science.1159699.

Bishop, J. L., M. D. Lane, M. D. Dyar, and A. J. Brown (2008b), Reflectance and emission spectroscopy study of four groups of phyllosilicates: Smectites, kaolinite-serpentines, chlorites and micas, *Clay Miner.*, *43*(1), 35–54, doi:10.1180/claymin.2008.043.1.03.

Borchardt, G. (1989), Smectites, *Miner. Soil Environ.*, *2*, 675–727.

Bourman, R. P., and C. D. Ollier (2002), A critique of the Schellmann definition and classification of "laterite,", *Catena*, *47*(2), 117–131, doi:10.1016/S0341-8162(01)00178-3.

Brimhall, G. H., and W. E. Dietrich (1987), Constitutive mass balance relations between chemical composition, volume, density, porosity, and strain in metasomatic hydrochemical systems: Results on weathering and pedogenesis, *Geochim. Cosmochim. Acta*, *51*(3), 567–587, doi:10.1016/0016-7037(87)90070-6.

Burns, R. G. (1981), Intervalence transitions in mixed-valence minerals of iron and titanium, *Annu. Rev. Earth Planet. Sci.*, *9*, 345–383, doi:10.1146/annurev.ea.09.050181.002021.

Burns, R. G. (1993), *Mineralogical Applications of Crystal Field Theory*, 2nd ed., 551 pp., Cambridge Univ. Press, Cambridge, U. K.

Carter, J., and F. Poulet (2012), Global investigation of hydrated exposures on Mars: Evidence for a clay cycle, *Lunar Planet. Sci.*, *XXXXIII*, Abstract 1436.

Chan, M. A., B. Beitler, W. T. Parry, J. Ormö, and G. Komatsu (2004), A possible terrestrial analogue for haematite concretions on Mars, *Nature*, *429*(6993), 731–734, doi:10.1038/nature02600.

Chemtob, S. M., B. L. Jolliff, G. R. Rossman, J. M. Eiler, and R. E. Arvidson (2010), Silica coatings in the Ka'u Desert, Hawaii, a Mars analog terrain: A micromorphological, spectral, chemical, and isotopic study, *J. Geophys. Res.*, *115*, E04001, doi:10.1029/2009JE003473.

Christensen, P. R., et al. (2000a), Detection of crystalline hematite mineralization on Mars by the Thermal Emission Spectrometer: Evidence for near-surface water, *J. Geophys. Res.*, *105*(E4), 9623–9642, doi:10.1029/1999JE001093.

Christensen, P. R., J. L. Bandfield, M. D. Smith, V. E. Hamilton, and R. N. Clark (2000b), Identification of a basaltic component on the Martian surface from Thermal Emission Spectrometer data, *J. Geophys. Res.*, *105*(E4), 9609–9621, doi:10.1029/1999JE001127.

Clark, R. N., T. V. V. King, M. Klejwa, G. A. Swayze, and N. Vergo (1990), High spectral resolution reflectance spectroscopy of minerals, *J. Geophys. Res.*, *95*(B8), 12,653–12,680, doi:10.1029/JB095iB08p12653.

Clark, R. N., G. A. Swayze, R. Wise, E. Livo, T. Hoefen, R. Kokaly, and S. J. Sutley (2007), USGS digital spectral library splib06a, *U.S. Geol. Surv. Digital Data Ser.*, *231*.

Cloutis, E. A., and M. J. Gaffey (1991), Pyroxene spectroscopy revisited: Spectral-compositional correlations and relationship to geothermometry, *J. Geophys. Res.*, *96*(E5), 22,809–22,826, doi:10.1029/91JE02512.

Cloutis, E. A., P. M. Asher, and S. A. Mertzman (2002), Spectral reflectance properties of zeolites and remote sensing implications, *J. Geophys. Res.*, *107*(E9), 5067, doi:10.1029/2000JE001467.

Crown, D. A., and C. M. Pieters (1987), Spectral properties of plagioclase and pyroxene mixtures and the interpretation of lunar soil spectra, *Icarus*, *72*(3), 492–506, doi:10.1016/0019-1035(87)90047-9.

Duchaufour, P., and B. Souchier (1978), Roles of iron and clay in Genesis of acid soils under a humid, temperate climate, *Geoderma*, *20*(1), 15–26, doi:10.1016/0016-7061(78)90046-0.

Ehlmann, B. L., et al. (2009), Identification of hydrated silicate minerals on Mars using MRO-CRISM: Geologic context near Nili Fossae and implications for aqueous alteration, *J. Geophys. Res.*, *114*, E00D08, doi:10.1029/2009JE003339.

Ehlmann, B. L., J. F. Mustard, S. L. Murchie, J.-P. Bibring, A. Meunier, A. A. Fraeman, and Y. Langevin (2011), Subsurface water and clay mineral formation during the early history of Mars, *Nature*, *479*(7371), 53–60, doi:10.1038/nature10582.

Ehlmann, B. L., D. L. Bish, S. W. Ruff, and J. F. Mustard (2012), Mineralogy and chemistry of altered Icelandic basalts: Application to clay mineral detection and understanding aqueous environments on Mars, *J. Geophys. Res.*, doi:10.1029/2012JE004156, in press.

Farmer, V. C. (1974), The layer silicates, in *The Infrared Spectra of Minerals*, edited by V. C. Farmer, pp. 331–363, Mineral. Soc., London.

Feely, K. C., and P. R. Christensen (1999), Quantitative compositional analysis using thermal emission spectroscopy: Application to igneous and metamorphic rocks, *J. Geophys. Res.*, *104*(E10), 24,195–24,210, doi:10.1029/1999JE001034.

Gaffey, M. J., J. F. Bell, R. H. Brown, T. H. Burbine, J. L. Piatek, K. L. Reed, and D. A. Chaky (1993), Mineralogical variations within the S-type asteroid class, *Icarus*, *106*(2), 573–602, doi:10.1006/icar.1993.1194.

Galan, E., P. Aparicio, I. Gonzalez, and A. Miras (1998), Contribution of multivariate analysis to the correlation of some properties of kaolin with its mineralogical and chemical composition, *Clay Miner.*, *33*(1), 65–75, doi:10.1180/000985598545435.

Gaudin, A., E. Dehouck, and N. Mangold (2011), Evidence for weathering on early Mars from a comparison with terrestrial weathering profiles, *Icarus*, *216*(1), 257–268, doi:10.1016/j.icarus.2011.09.004.

Gavin, P., V. F. Chevrier, M. R. G. Sayyed, and R. Islam (2012), Spectral analysis of deccan intrabasaltic bole beds: Implications for phyllosilicate formation on Mars, *Lunar Planet. Sci.*, *XXXXIII*, Abstract 1621.

Goldich, S. S. (1938), A study in rock-weathering, *J. Geol.*, *46*(1), 17–58, doi:10.1086/624619.

Hamilton, V. E. (2000), Thermal infrared emission spectroscopy of the pyroxene mineral series, *J. Geophys. Res.*, *105*(E4), 9701–9716, doi:10.1029/1999JE001112.

Hapke, B. (1981), Bidirectional reflectance spectroscopy 1. Theory, *J. Geophys. Res.*, *86*(B4), 3039–3054, doi:10.1029/JB086iB04p03039.

Hausrath, E. M., A. K. Navarre-Sitchler, P. B. Sak, C. I. Steefel, and S. L. Brantley (2008a), Basalt weathering rates on Earth and the duration of liquid water on the plains of Gusev Crater, Mars, *Geology*, *36*(1), 67–70, doi:10.1130/G24238A.1.

Hausrath, E. M., A. H. Treiman, E. Vicenzi, D. L. Bish, D. Blake, P. Sarrazin, T. Hoehler, I. Midtkandal, A. Steele, and S. L. Brantley (2008b), Short- and long-term olivine weathering in svalbard: Implications for Mars, *Astrobiology*, *8*(6), 1079–1092, doi:10.1089/ast.2007.0195.

Hill, I. G., R. H. Worden, and I. G. Meighan (2000), Geochemical evolution of a palaeolaterite: The Interbasaltic Formation, Northern Ireland, *Chem. Geol.*, *166*(1–2), 65–84, doi:10.1016/S0009-2541(99)00179-5.

Howard, A. D., and J. M. Moore (2007), The Light-toned Sediments in and near Lower Mawrth Vallis May be a Drape Deposit, *Lunar Planet. Sci.*, *XXXVIII*, Abstract 1339.

Iriarte, I., S. Petit, F. J. Huertas, S. Fiore, O. Grauby, A. Decarreau, and J. Linares (2005), Synthesis of kaolinite with a high level of Fe3+ for al substitution, *Clays Clay Miner.*, *53*(1), 1–10, doi:10.1346/CCMN.2005.0530101.

Jackson, M. L., and G. D. Sherman (1953), Chemical weathering of minerals in soils, *Adv. Agron.*, *5*, 219–318, doi:10.1016/S0065-2113(08)60231-X.

Jay, A. E., and M. Widdowson (2008), Stratigraphy, structure and volcanology of the SE Deccan continental flood basalt province: Implications for eruptive extent and volumes, *J. Geol. Soc.*, *165*(1), 177–188, doi:10.1144/0016-76492006-062.

Jin, L., R. Ravella, B. Ketchum, P. R. Bierman, P. Heaney, T. White, and S. L. Brantley (2010), Mineral weathering and elemental transport during hillslope evolution at the Susquehanna/Shale Hills Critical Zone Observatory, *Geochim. Cosmochim. Acta*, *74*(13), 3669–3691, doi:10.1016/j.gca.2010.03.036.

Kısakürek, B., M. Widdowson, and R. H. James (2004), Behaviour of Li isotopes during continental weathering: The Bidar laterite profile, India, *Chem. Geol.*, *212*(1–2), 27–44, doi:10.1016/j.chemgeo.2004.08.027.

Loizeau, D., et al. (2007), Phyllosilicates in the Mawrth Vallis region of Mars, *J. Geophys. Res.*, *112*, E08S08, doi:10.1029/2006JE002877. E08S04

Mangold, N., et al. (2007), Mineralogy of the Nili Fossae region with OMEGA/Mars Express data: 2. Aqueous alteration of the crust, *J. Geophys. Res.*, *112*, E08S04, doi:10.1029/2006JE002835.

McCord, T. B., J. B. Adams, and T. V. Johnson (1970), Asteroid Vesta: Spectral reflectivity and compositional implications, *Science*, *168*(3938), 1445–1447, doi:10.1126/science.168.3938.1445.

McKeown, N. K., J. L. Bishop, E. Z. N. Dobrea, B. L. Ehlmann, M. Parente, J. F. Mustard, S. L. Murchie, G. A. Swayze, J.-P. Bibring, and E. A. Silver (2009), Characterization of phyllosilicates observed in the central Mawrth Vallis region, Mars, their potential formational processes, and implications for past climate, *J. Geophys. Res.*, *114*, E00D10, doi:10.1029/2008JE003301.

Merino, E., D. Nahon, and Y. Wang (1993), Kinetics and mass transfer of pseudomorphic replacement; application to replacement of parent minerals and kaolinite by Al, Fe, and Mn oxides during weathering, *Am. J. Sci.*, *293*(2), 135–155, doi:10.2475/ajs.293.2.135.

Michalski, J. R., and P. B. Niles (2011), Formation of jarosite in the Mawrth Vallis region of Mars by weathering within paleo-ice deposits, *Lunar Planet. Sci.*, *XXXXII*, Abstract 1926.

Michalski, J. R., and E. Z. Noe Dobrea (2007), Evidence for a sedimentary origin of clay minerals in the Mawrth Vallis region, Mars, *Geology*, *35*(10), 951–954, doi:10.1130/G23854A.1.

Michalski, J. R., M. D. Kraft, T. G. Sharp, L. B. Williams, and P. R. Christensen (2005), Mineralogical constraints on the high-silica Martian surface component observed by TES, *Icarus*, *174*(1), 161–177, doi:10.1016/j.icarus.2004.10.022.

Michalski, J. R., M. D. Kraft, T. G. Sharp, and P. R. Christensen (2006), Effects of chemical weathering on infrared spectra of Columbia River Basalt and spectral interpretations of Martian alteration, *Earth Planet. Sci. Lett.*, *248*(3–4), 822–829, doi:10.1016/j.epsl.2006.06.034.

Milliken, R. E., and D. L. Bish (2010), Sources and sinks of clay minerals on Mars, *Philos. Mag.*, *90*(17–18), 2293–2308, doi:10.1080/14786430903575132.

Milliken, R. E., D. L. Bish, T. Bristow, and J. F. Mustard (2010), The case for mixed-layered clays on Mars, *Lunar Planet. Sci.*, *XXXXI*, Abstract 2030.

Ming, D. W., and F. A. Mumpton (1989), Zeolites in soils, in *Minerals in Soil Environments*, 2nd ed., pp. 873–911, Soil Sci. Soc. of Am., Madison, Wis.

Minitti, M. E., C. M. Weitz, M. D. Lane, and J. L. Bishop (2007), Morphology, chemistry, and spectral properties of Hawaiian rock coatings and implications for Mars, *J. Geophys. Res.*, *112*, E05015, doi:10.1029/2006JE002839.

Murchie, S., et al. (2007), Compact Reconnaissance Imaging Spectrometer for Mars (CRISM) on Mars Reconnaissance Orbiter (MRO), *J. Geophys. Res.*, *112*, E05S03, doi:10.1029/2006JE002682.

Murchie, S. L., et al. (2009), A synthesis of Martian aqueous mineralogy after 1 Mars year of observations from the Mars Reconnaissance Orbiter, *J. Geophys. Res.*, *114*, E00D06, doi:10.1029/2009JE003342.

Murray, R., D. J. Miller, and K. Kryc (2000), Analysis of major and trace elements in rocks, sediments, and interstitial waters by inductively coupled plasma–atomic emission spectrometry (ICP-AES), *ODP Tech. Note*, *29*, 1–27.

Mustard, J., and J. Hays (1997), Effects of hyperfine particles on reflectance spectra from 0.3 to 25 $\mu$m, *Icarus*, *125*(1), 145–163, doi:10.1006/icar.1996.5583.

Mustard, J. F., et al. (2008), Hydrated silicate minerals on Mars observed by the Mars Reconnaissance Orbiter CRISM instrument, *Nature*, *454*(7202), 305–309, doi:10.1038/nature07097.

Nash, D. B., and J. W. Salisbury (1991), Infrared reflectance spectra (2.2–15 $\mu$m) of plagioclase feldspars, *Geophys. Res. Lett.*, *18*(6), 1151–1154, doi:10.1029/91GL01008.

Nesbitt, H. W., and R. E. Wilson (1992), Recent chemical weathering of basalts, *Am. J. Sci.*, *292*(10), 740–777, doi:10.2475/ajs.292.10.740.

Nesbitt, H. W., and G. M. Young (1989), Formation and diagenesis of weathering profiles, *J. Geol.*, *97*(2), 129–147, doi:10.1086/629290.

Niles, P. B., and J. Michalski (2009a), Linking sulfate and phyllosilicate formation at Mawrth Vallis: Weathering in ancient low-latitude ice deposits, *Eos Trans. AGU*, *90*(52), Fall Meet. Suppl., Abstract P12A-05.

Niles, P. B., and J. Michalski (2009b), Meridiani Planum sediments on Mars formed through weathering in massive ice deposits, *Nat. Geosci.*, *2*(3), 215–220, doi:10.1038/ngeo438.

Noe Dobrea, E. Z., et al. (2010), Mineralogy and stratigraphy of phyllosilicate-bearing and dark mantling units in the greater Mawrth Vallis/west Arabia Terra area: Constraints on geological origin, *J. Geophys. Res.*, *115*, E00D19, doi:10.1029/2009JE003351.

Ollier, C. D., and H. C. Sheth (2008), The High Deccan duricrusts of India and their significance for the "laterite" issue, *J. Earth Syst. Sci.*, *117*(5), 537–551, doi:10.1007/s12040-008-0051-9.

Pain, C. F., and C. D. Oilier (1995), Inversion of relief—A component of landscape evolution, *Geomorphology*, *12*(2), 151–165, doi:10.1016/0169-555X(94)00084-5.

Pande, K. (2002), Age and duration of the Deccan Traps, India A review of radiometric and paleomagnetic constraints, *J. Earth Syst. Sci.*, *111*(2), 115, doi:10.1007/BF02981139.

Pate, J. S., W. H. Verboom, and P. D. Galloway (2001), TURNER REVIEW No. 4. Co-occurrence of Proteaceae, laterite and related oligotrophic soils: Coincidental associations or causative inter-relationships?, *Aust. J. Bot.*, *49*(5), 529–560, doi:10.1071/BT00086.

Petit, S., J. Madejova, A. Decarreau, and F. Martin (1999), Characterization of octahedral substitutions in kaolinites using near infrared spectroscopy, *Clays Clay Miner.*, *47*(1), 103–108, doi:10.1346/CCMN.1999.0470111.

Pieters, C. M. (1983), Strength of mineral absorption features in the transmitted component of near-infrared reflected light: First results from RELAB, *J. Geophys. Res.*, *88*(B11), 9534–9544, doi:10.1029/JB088iB11p09534.

Poulet, F., N. Mangold, D. Loizeau, J.-P. Bibring, Y. Langevin, J. Michalski, and B. Gondet (2008), Abundance of minerals in the phyllosilicate-rich units on Mars, *Astron. Astrophys.*, *487*(2), L41–L44, doi:10.1051/0004-6361:200810150.

Rai, D., and J. A. Kittrick (1989), Mineral equilibria and the soil system, in *Mineral in Soil Environments*, *Soil Sci. Soc. Am. Book Ser.*, *2*, 161–198.

Righi, D., and A. Meunier (1995), Origin of clays by rock weathering, in *Origin and Mineralogy of Clays*, pp. 43–161, Springer, Berlin.

Salisbury, J. W., and L. S. Walter (1989), Thermal infrared (2.5–13.5 $\mu$m) spectroscopic remote sensing of igneous rock types on particulate planetary surfaces, *J. Geophys. Res.*, *94*(B7), 9192–9202, doi:10.1029/JB094iB07p09192.

Salisbury, J. W., A. Wald, and D. M. D'Aria (1994), Thermal-infrared remote sensing and Kirchhoff's law 1. Laboratory measurements, *J. Geophys. Res.*, *99*(B6), 11,897–11,911, doi:10.1029/93JB03600.

Scheinost, A. C., A. Chavernas, V. Barron, and J. Torrent (1998), Use and limitations of second-derivative diffuse reflectance spectroscopy in the visible to near-infrared range to identify and quantify Fe oxide minerals in soils, *Clays Clay Miner.*, *46*(5), 528–536, doi:10.1346/CCMN.1998.0460506.

Schellmann, W. (1981), Considerations on the definition and classification of laterites, in *Proceedings of the International Seminar on Lateritisation Processes, Trivandrum, India*, vol. 47, pp. 117–131, A. A. Balkema, Rotterdam, Netherlands.

Schmidt, P. W., V. Prasad, and P. K. Ramam (1983), Magnetic ages of some Indian laterites, *Palaeogeogr. Palaeoclimatol. Palaeoecol.*, *44*(3–4), 185–202, doi:10.1016/0031-0182(83)90102-5.

Schwenzer, S. P., and D. A. Kring (2009), Impact-generated hydrothermal systems capable of forming phyllosilicates on Noachian Mars, *Geology*, *37*(12), 1091–1094, doi:10.1130/G30340A.1.

Seelos, K. D., R. E. Arvidson, B. L. Jolliff, S. M. Chemtob, R. V. Morris, D. W. Ming, and G. A. Swayze (2010), Silica in a Mars analog environment: Ka'u Desert, Kilauea Volcano, Hawaii, *J. Geophys. Res.*, *115*, E00D15, doi:10.1029/2009JE003347.

Sherman, D. M., and T. D. Waite (1985), Electronic spectra of Fe (super 3+) oxides and oxide hydroxides in the near IR to near UV, *Am. Mineral.*, *70*(11–12), 1262–1269.

Strens, R. G. J. (1974), The common chain, ribbon, and ring silicates, in *The Infrared Spectra of Minerals*, edited by V. C. Farmer, pp. 305–330, Mineral. Soc., London.

Stubican, V., and R. Roy (1961), Isomorphous substitution and infra-red spectra of the layer lattice silicates, *Am. Mineral.*, *46*, 32–51.

Taylor, G., R. A. Eggleton, C. C. Holzhauer, L. A. Maconachie, M. Gordon, M. C. Brown, and K. G. McQueen (1992), Cool climate lateritic and bauxitic weathering, *J. Geol.*, *100*(6), 669–677, doi:10.1086/629620.

Vandenberghe, R. E., E. De Grave, and P. M. A. de Bakker (1994), On the methodology of the analysis of Mössbauer spectra, *Hyperfine Interact.*, *83*(1), 29–49, doi:10.1007/BF02074257.

White, A. F. (1995), Chemical weathering rates of silicate minerals in soils, *Rev. Mineral. Geochem.*, *31*(1), 407–461.

Widdowson, M., and K. G. Cox (1996), Uplift and erosional history of the Deccan Traps, India: Evidence from laterites and drainage patterns of the Western Ghats and Konkan Coast, *Earth Planet. Sci. Lett.*, *137*(1–4), 57–69, doi:10.1016/0012-821X(95)00211-T.

Widdowson, M., J. N. Walsh, and K. V. Subbarao (1997), The geochemistry of Indian bole horizons: Palaeoenvironmental implications of Deccan intravolcanic palaeosurfaces, *Geol. Soc. Spec. Publ.*, *120*(1), 269–281, doi:10.1144/GSL.SP.1997.120.01.17.

Wilson, M. J. (1999), The origin and formation of clay minerals in soils; past, present and future perspectives, *Clay Miner.*, *34*(1), 7–25, doi:10.1180/000985599545957.

Wilson, M. J. (2004), Weathering of the primary rock-forming minerals: Processes, products and rates, *Clay Miner.*, *39*(3), 233–266, doi:10.1180/0009855043930133.

Wimpenny, J., A. Gannoun, K. W. Burton, M. Widdowson, R. H. James, and S. R. Gíslason (2007), Rhenium and osmium isotope and elemental behaviour accompanying laterite formation in the Deccan region of India, *Earth Planet. Sci. Lett.*, *261*(1–2), 239–258, doi:10.1016/j.epsl.2007.06.028.

Wray, J. J., B. L. Ehlmann, S. W. Squyres, J. F. Mustard, and R. L. Kirk (2008), Compositional stratigraphy of clay-bearing layered deposits at Mawrth Vallis, Mars, *Geophys. Res. Lett.*, *35*, L12202, doi:10.1029/2008GL034385.

Wray, J. J., S. L. Murchie, S. W. Squyres, F. P. Seelos, and L. L. Tornabene (2009), Diverse aqueous environments on ancient Mars revealed in the southern highlands, *Geology*, *37*(11), 1043–1046, doi:10.1130/G30331A.1.

Wyatt, M. B., V. E. Hamilton, H. Y. M. Jr, P. R. Christensen, and L. A. Taylor (2001), Analysis of terrestrial and Martian volcanic compositions using thermal emission spectroscopy: 1. Determination of mineralogy, chemistry, and classification strategies, *J. Geophys. Res.*, *106*(E7), 14,711–14,732, doi:10.1029/2000JE001356.

Young, R. A. (1995), The Rietveld Method, *Int. Union Crystallogr. Monogr. Crystallogr.*, *5*, 298 pp.

Ziegler, K., J. C. C. Hsieh, O. A. Chadwick, E. F. Kelly, D. M. Hendricks, and S. M. Savin (2003), Halloysite as a kinetically controlled end product of arid-zone basalt weathering, *Chem. Geol.*, *202*(3–4), 461–478, doi:10.1016/j.chemgeo.2002.06.001.